of cancer patients. As with other oligonucleotide-based therapies, realizing the potential of therapeutic miRNAs will require an effective delivery technology. In a previous study, we showed that intravenous injections of EZH2 and p110α siRNA complexed with atelocollagen inhibited the tumor growth in bone tissues of the mouse model.[13] These results showed that an atelocollagen-mediated systemic delivery of siRNA could reach tumor cells at metastatic sites and inhibit tumor growth *in vivo*. As demonstrated here, atelocollagen facilitates the accumulation of enough synthetic miRNA in the cancers cells of an existing prostate tumor to affect the expression of a target gene. Furthermore, the combination of synthetic miR-16 and atelocollagen strongly inhibited the development of human prostate tumors in the bones of mice. Interestingly, the effect of miR-16 appeared to be restricted to the prostate cancer cells, as the miR-16 treated mice showed no notable side effects. Follow-up studies featuring the treatment of larger tumors and more extensive toxicity studies will be required to demonstrate the therapeutic potential of atelocollagen-miR-16; however, these early results are extremely encouraging.

MATERIALS AND METHODS

Cell culture. The human prostate cell line 22Rv1, LNCaP, DU145, and PPC-1 cells were obtained from American Type Culture Collection (Manassas, VA) and maintained in RPMI 1640 medium containing 10% fetal bovine serum. The PC-3M-luc cells continuously expressing firefly luciferase (Xenogen, Alameda, CA) were maintained in RPMI 1640 medium supplemented with 10% fetal bovine serum and 0.2 mg/ml zeocin (Invitrogen, Carlsbad, CA). For construction of 3′-UTR–renilla luciferase plasmid and reporter assays, the segment of 3′-UTR of *Bcl2* gene was amplified by PCR using genomic DNA from normal human prostate epithelial cells (CT-2555; Lonza Walkersville, Walkersville, MD) as reported.[17] The PCR product was inserted into the pGL4.75[HRuc/CMV] vector (Promega, Madison, WI), using *XbaI* site immediately downstream from the stop codon of renilla luciferase (pGL4.75[HRuc/CMV]-Bcl2 3′UTR). For reporter assays, PC-3M-luc-C6 cells were transfected with 2 μg of pGL4.75[HRuc/CMV]-Bcl2 3′UTR using LipofectAMINE 2000 (Invitrogen). Stable transfectants were selected in hygromycine (0.2 mg/ml; Invitrogen) and bioluminescence was used to screen transfected clones for renilla and firefly luciferase gene expression using dual-luciferase assay system (Promega), intensity of renilla luciferase was normalized by firefly luciferase. Clones expressing the both luciferase gene were named PC-3M-luc/Rluc-Bcl2 3′UTR. The cells were maintained *in vitro* at 37 °C in a humidified atmosphere of 5% CO_2.

Transfection with synthetic miR-16 and assay of cellular proliferation. Synthetic hsa-miR-16 (Pre-miR-hsa-miR-16; Ambion, Austin, TX) or NC miRNA (Pre-miR microRNA Precursor Molecule-Negative Control #2, cat. no. AM17111; Ambion) was delivered via lipid-based reverse transfection with 30 nmol/l final concentration of miRNA as described previously.[29] As a control for inhibition of cellular proliferation, siRNA against the motor protein kinesin 11, also known as Eg5, was used. Eg5 is essential for cellular survival of most eukaryotic cells and a lack thereof leads to reduced cell proliferation and cell death.[30] siEg5 was used in lipid-based transfection following the same experimental parameters that apply to miRNA. We observed 50–70% growth inhibition in all cell lines used in this study. Percent (%) proliferation values from the alamar blue assay (Invitrogen) were normalized to values from cells treated with NC miRNA.

Quantitative RT-PCR of miR-16. Human cultured cell line RNA was isolated using the ISOGEN (Wako Chemical, Tokyo, Japan). MiRNA-specific complementary DNA was generated using the TaqMan MicroRNA RT Kit (Applied Biosystems, Foster City, CA) and the miRNA-specific RT primer from the TaqMan Micro RNA Assay (Applied Biosystems). The expression of the U6 small nuclear RNA was used as an internal normalization control. miRNA levels were also measured by using the miRNA-specific probe included with TaqMan Micro RNA Assay on a Real-Time PCR System 7300 and SDS software (Applied Biosystems).

Quantitative PCR of miR-16 loci on chromosome 13q14. Genomic DNAs were extracted from PC-3M-luc and prostate epithelial cells using DNAeasy (Qiagen, Valencia, CA). Quantitative PCR for the miR-16 loci on chromosome 13q14 was performed using Platinum SYBR Green qPCR SuperMix-UDG (Invitrogen) and primer sequences were 5′-GCA GCA CAG TTA ATA CTG GA-3′ and 5′-ATA GCT CTT ATG ATA GCA AT-3′. The house keeping gene, *RNase P* was also quantified as a control reference gene using Platinum Quantitative PCR SuperMix-UDG (Invitrogen) and TaqMan RNase P Detection Reagents Kit (Applied Biosystems). The reactions were incubated at 50 °C for 2 minutes, then heated to 95 °C for 2 minutes followed by 45 cycles of 15 seconds at 95 °C, and 30 seconds at 60 °C.

Evaluation of miRNA delivery to bone-metastatic tumors in mice. Animal experiments in this study were performed in compliance with the guidelines of the Institute for Laboratory Animal Research, National Cancer Center Research Institute. Seven- to ten-week-old male Balb/c athymic nude mice (CLEA Japan, Shizuoka, Japan) were anesthetized by exposure to 3% isoflurane on day zero and subsequent days. On day zero of the experiments, to generate a bone-metastatic human prostate cancer model, the anesthetized animals were injected with 2×10^6 PC-3M-luc/Rluc-Bcl2 3′UTR cells suspended in 100 μl sterile Dulbecco's phosphate-buffered saline into the left heart ventricle.[13,15,16] For *in vivo* imaging, the mice were injected with ViviRen (5 mg/kg; Promega) by intravenous tail vein injection and imaged immediately to count the photons from animal whole bodies using the IVIS imaging system (Xenogen). After the bioluminescence from renilla luciferase disappeared, photons from firefly luciferase were counted as described previously.[13]

Preparation of complex with miR-16 and atelocollagen. For preparing the complexes of miRNA and atelocollagen (Koken, Tokyo, Japan), an equal volume of atelocollagen (0.1 % in phosphate-buffered saline at pH 7.4) and miRNA solution were combined and mixed by rotating for 1 hour at 4 °C. The final concentration of atelocollagen was 0.05%. Nine weeks after tumor injection, individual mice (from cohorts containing three animals) were injected with 200 μl of atelocollagen containing 50 μg of miR-16 complexed with atelocollagen, or NC miRNA/atelocollagen by intravenous tail-vein injection.

Analysis of miR-16/atelocollagen treatment for bone-metastatic prostate cancer. Mice were inoculated with PC-3M-luc cells into the left cardiac ventricle on day zero as described previously.[13] The miR-16 and NC miRNA (50 μg) with 0.05% atelocollagen in a 200 μl volume were injected into the mouse tail vein on days 4, 7, and 10 postinoculation. Each experimental condition included six animals per group. At the end of the experiment on day 28, to confirm the presence of neoplastic cells, selected tissues were excised from the mice at necropsy. Tissues were fixed in 4% formaldehyde-phosphate-buffered saline(–), embedded in paraffin, cut into 5-μm sections, and stained with hematoxylin and eosin.

Clinical samples. Human prostate tissue samples derived from resected prostates from treatment-naive men with an average age of 65 (range of 52–76) diagnosed with nonmetastatic T2 or T3 prostate adenocarcinoma who gave informed consent. Gleason scores for all patients were 8 or 9. The tissues from patients were formalin-fixed, paraffin-embedded, sectioned, hematoxylin and eosin stained, and subjected to microscopic analysis. Three adjacent sections comprising 60–90% (74% average) cancerous tissue were selected as cancer samples from each patient. Three adjacent sections lacking evidence of cancer cells were selected as normal adjacent

samples. RNA from the tissues were prepared using the RecoverAll Total RNA Isolation Kit (Ambion). The isolated RNA was subjected to qRT-PCR for miR-16 as described above.

MiR-16 functional pathway analysis. For preparation of RNA samples, PC-3M-luc cells were reverse transfected in quadruplicate by complexing miR-16 and NC miRNA and NeoFX transfection reagent (Ambion). The final concentration of miRNA was 30 nmol/l. Cells were harvested at 72 hours post-transfection. One microgram of total RNA per sample was used to prepare biotin-labeled cRNA using a MessageAmp II-based protocol (Ambion) and one round of amplification. Labeled cRNA was hybridized, washed, and scanned using Illumina's recommended protocols. Illumina BeadScan software was used to produce .idat, .xml, and .tif files for each array on a slide. Raw data were extracted using Illumina BeadStudio software, v 3.0 (Illumina, San Diego, CA). Following quality assessment, data from the replicate beads on each array were summarized into average intensity values and variances. The background subtracted data were used to compare the relative expression of mRNAs in cells transfected with miR-16, NC miRNA, and transfection agent only. analysis of variance was used to judge the significance of the variation observed between the various treatment groups. In total, 285 mRNAs exceeded the thresholds used to identify differentially expressed genes (log ratio greater than 0.5 or less than −0.5 for the average signal between miR-16 and NC miRNA or transfection agent only treatments and P values <0.001 for the 72 hour time-point).

Statistical analysis. The results are given as mean ± SD Statistical analysis was conducted using the analysis of variance with the Bonferroni correction for multiple comparisons. A P value of ≤0.05 was considered to indicate a significant difference.

SUPPLEMENTARY MATERIAL

Figure S1. The scheme of dual luciferase assay for monitoring of systemic miR-16 delivery.

Figure S2. Overview of experimental protocol for inhibition of metastatic tumor growth in bone tissues by the atelocollagen-mediated miRNA treatment.

Figure S3. KEGG cell cycle diagram.

Table S1. Data of the mRNA array for comparison of miR-16 and NC miR transfected PC-3M-luc cells.

ACKNOWLEDGMENTS

We thank Ayako Inoue, Ayano Matsumoto, and Maho Kodama for their excellent technical work. We also thank Shunji Nagahara of Formulation Research Laboratories, Technology Research and Development Center, Dainippon Sumitomo Pharma Co., Ltd. for technological support and Koken Co., Ltd. for providing atelocollagen. This work was supported in part by a Grant-in-Aid for the Third-Term Comprehensive 10-Year Strategy for Cancer Control, a Grant-in-Aid for Scientific Research on Priority Areas Cancer from the Ministry of Education, Culture, Sports, Science and Technology, and the Program for Promotion of Fundamental Studies in Health Sciences of the National Institute of Biomedical Innovation (NiBio), and a Takeda Science Foundation.

REFERENCES

1. Calin, GA, Sevignani, C, Dumitru, CD, Hyslop, T, Noch, E, Yendamuri, S *et al.* (2004). Human microRNA genes are frequently located at fragile sites and genomic regions involved in cancers. *Proc Natl Acad Sci USA* **101**: 2999–3004.
2. Calin, GA, Ferracin, M, Cimmino, A, Di Leva, G, Shimizu, M, Wojcik, SE *et al.* (2005). A microRNA signature associated with prognosis and progression in chronic lymphocytic leukemia. *N Engl J Med* **353**: 1793–1801.
3. Calin, GA and Croce, CM (2006). MicroRNA-cancer connection: the beginning of a new tale. *Cancer Res* **66**: 7390–7394.
4. Lu, J, Getz, G, Miska, EA, Alvarez-Saavedra, E, Lamb, J, Peck, D *et al.* (2005). MicroRNA expression profiles classify human cancers. *Nature* **435**: 834–838.
5. Volinia, S, Calin, GA, Liu, CG, Ambs, S, Cimmino, A, Petrocca, F *et al.* (2006). A microRNA expression signature of human solid tumors defines cancer gene targets. *Proc Natl Acad Sci USA* **103**: 2257–2261.
6. Mattie, MD, Benz, CC, Bowers, J, Sensinger, K, Wong, L, Scott, GK *et al.* (2006). Optimized high-throughput microRNA expression profiling provides novel biomarker assessment of clinical prostate and breast cancer biopsies. *Mol Cancer* **5**: 24.
7. Porkka, KP, Pfeiffer, MJ, Waltering, KK, Vessella, RL, Tammela, TL and Visakorpi, T (2007). MicroRNA expression profiling in prostate cancer. *Cancer Res* **67**: 6130–6135.
8. Bonci, D, Coppola, V, Musumeci, M, Addario, A, Giuffrida, R, Memeo, L *et al.* (2008). The miR-15a-miR-16-1 cluster controls prostate cancer by targeting multiple oncogenic activities. *Nat Med* **14**: 1271–1277.
9. Bullrich, F and Croce, CM (2001). Molecular biology of chronic lymphocytic leukemia. In: Cheson, B (ed.). *Chronic Lymphoid Leukemia*. Dekker: New York, pp. 9–32.
10. Dong, JT, Boyd, JC and Frierson, HF (2001). Loss of heterozygosity at 13q14 and 13q21 in high grade, high stage prostate cancer. *Prostate* **49**: 166–171.
11. Calin, GA, Dumitru, CD, Shimizu, M, Bichi, R, Zupo, S, Noch, E *et al.* (2002). Frequent deletions and down-regulation of micro-RNA genes miR15 and miR16 at 13q14 in chronic lymphocytic leukemia. *Proc Natl Acad Sci USA* **99**: 15524–15529.
12. Calin, GA and Croce, CM (2006). Genomics of chronic lymphocytic leukemia microRNAs as new players with clinical significance. *Semin Oncol* **33**: 167–173.
13. Takeshita, F, Minakuchi, Y, Nagahara, S, Honma, K, Sasaki, H, Hirai, K *et al.* (2005). Efficient delivery of small interfering RNA to bone-metastatic tumors by using atelocollagen *in vivo*. *Proc Natl Acad Sci USA* **102**: 12177–12182.
14. Yin, Z, Spitz, MR, Babaian, RJ, Strom, SS, Troncoso, P and Kagan, J (1999). Limiting the location of a putative human prostate cancer tumor suppressor gene at chromosome 13q14.3. *Oncogene* **18**: 7576–7583.
15. Arguello, F, Furlanetto, RW, Baggs, RB, Graves, BT, Harwell, SE, Cohen, HJ *et al.* (1992). Incidence and distribution of experimental metastases in mutant mice with defective organ microenvironments (genotypes Sl/Sld and W/Wv). *Cancer Res* **52**: 2304–2309.
16. Jenkins, DE, Yu, SF, Hornig, YS, Purchio, T and Contag, PR (2003). *In vivo* monitoring of tumor relapse and metastasis using bioluminescent PC-3M-luc-C6 cells in murine models of human prostate cancer. *Clin Exp Metastasis* **20**: 745–756.
17. Cimmino, A, Calin, GA, Fabbri, M, Iorio, MV, Ferracin, M, Shimizu, M *et al.* (2005). miR-15 and miR-16 induce apoptosis by targeting BCL2. *Proc Natl Acad Sci USA* **102**: 13944–13949.
18. Johnson, CD, Esquela-Kerscher, A, Stefani, G, Byrom, M, Kelnar, K, Ovcharenko, D *et al.* (2007). The let-7 microRNA represses cell proliferation pathways in human cells. *Cancer Res* **67**: 7713–7722.
19. Kanehisa, M, Araki, M, Goto, S, Hattori, M, Hirakawa, M, Itoh, M *et al.* (2008). KEGG for linking genomes to life and the environment. *Nucleic Acids Res* **36**(Database issue): D480–D484.
20. Kanehisa, M and Goto, S (2000). KEGG: Kyoto Encyclopedia of Genes and Genomes. *Nucleic Acids Res* **28**: 27–30.
21. Kanehisa, M, Goto, S, Hattori, M, Aoki-Kinoshita, KF, Itoh, M, Kawashima, S *et al.* (2006). From genomics to chemical genomics: new developments in KEGG. *Nucleic Acids Res* **34**(Database issue): D354–D357.
22. Dennis, G, Sherman, BT, Hosack, DA, Yang, J, Gao, W, Lane, HC *et al.* (2003). DAVID: Database for Annotation, Visualization, and Integrated Discovery. *Genome Biol* **4**: P3.
23. Lu, W, Takahashi, H, Furusato, M, Maekawa, S, Nakano, M, Meng, C *et al.* (2006). Allelotyping analysis at chromosome 13q of high-grade prostatic intraepithelial neoplasia and clinically insignificant and significant prostate cancers. *Prostate* **66**: 405–412.
24. Chan, JA, Krichevsky, AM and Kosik, KS (2005). MicroRNA-21 is an antiapoptotic factor in human glioblastoma cells. *Cancer Res* **65**: 6029–6033.
25. Cheng, AM, Byrom, MW, Shelton, J and Ford, LP (2005). Antisense inhibition of human miRNAs and indications for an involvement of miRNA in cell growth and apoptosis. *Nucleic Acids Res* **33**: 1290–1297.
26. Johnson, SM, Grosshans, H, Shingara, J, Byrom, M, Jarvis, R, Cheng, A *et al.* (2005). RAS is regulated by the let-7 microRNA family. *Cell* **120**: 635–647.
27. Lim, LP, Lau, NC, Garrett-Engele, P, Grimson, A, Schelter, JM, Castle, J *et al.* (2005). Microarray analysis shows that some microRNAs downregulate large numbers of target mRNAs. *Nature* **433**: 769–773.
28. Lewis, BP, Burge, CB and Bartel, DP (2005). Conserved seed pairing, often flanked by adenosines, indicates that thousands of human genes are microRNA targets. *Cell* **120**: 15–20.
29. Ovcharenko, D, Jarvis, R, Hunicke-Smith, S, Kelnar, K and Brown, D (2005). High-throughput RNAi screening *in vitro*: from cell lines to primary cells. *RNA* **11**: 985–993.
30. Weil, D, Garçon, L, Harper, M, Duménil, D, Dautry, F and Kress, M (2002). Targeting the kinesin Eg5 to monitor siRNA transfection in mammalian cells. *BioTechniques* **33**: 1244–1248.

Leukemia (2009) 23, 2197–2209

www.nature.com/leu

LEADING ARTICLE

Mixed-lineage-leukemia (*MLL*) fusion protein collaborates with Ras to induce acute leukemia through aberrant *Hox* expression and Raf activation

R Ono[1,2,3], H Kumagai[1], H Nakajima[4,5], A Hishiya[1,2], T Taki[6], K Horikawa[7], K Takatsu[7,8], T Satoh[9], Y Hayashi[10], T Kitamura[2] and T Nosaka[1,2,3]

[1]*Division of Hematopoietic Factors, The Institute of Medical Science, The University of Tokyo, Tokyo, Japan;* [2]*Division of Cellular Therapy, The Institute of Medical Science, The University of Tokyo, Tokyo, Japan;* [3]*Department of Microbiology and Molecular Genetics, Mie University Graduate School of Medicine, Mie, Japan;* [4]*Center of Excellence, The Institute of Medical Science, The University of Tokyo, Tokyo, Japan;* [5]*Division of Hematology, Department of Internal Medicine, Keio University School of Medicine, Tokyo, Japan;* [6]*Department of Molecular Laboratory Medicine, Kyoto Prefectural University of Medicine Graduate School of Medical Science, Kamigyo-ku, Kyoto, Japan;* [7]*Department of Immunology, The Institute of Medical Science, The University of Tokyo, Tokyo, Japan;* [8]*Department of Immunobiology and Pharmaceutical Genetics, Graduate School of Medicine and Pharmaceutical Sciences, University of Toyama, Toyama, Japan;* [9]*Division of Molecular Biology, Department of Biochemistry and Molecular Biology, Kobe University Graduate School of Medicine, Kobe, Japan and* [10]*Gunma Children's Medical Center, Gunma, Japan*

***Mixed-lineage-leukemia* (*MLL*) fusion oncogenes are closely involved in infant acute leukemia, which is frequently accompanied by mutations or overexpression of *FMS-like receptor tyrosine kinase 3* (*FLT3*). Earlier studies have shown that *MLL* fusion proteins induced acute leukemia together with another mutation, such as an *FLT3* mutant, in mouse models. However, little has hitherto been elucidated regarding the molecular mechanism of the cooperativity in leukemogenesis. Using murine model systems of the *MLL*-fusion-mediated leukemogenesis leading to oncogenic transformation *in vitro* and acute leukemia *in vivo*, this study characterized the molecular network in the cooperative leukemogenesis. This research revealed that *MLL* fusion proteins cooperated with activation of Ras *in vivo*, which was substitutable for Raf *in vitro*, synergistically, but not with activation of signal transducer and activator of transcription 5 (STAT5), to induce acute leukemia *in vivo* as well as oncogenic transformation *in vitro*. Furthermore, *Hoxa9*, one of the *MLL*-targeted critical molecules, and activation of Ras *in vivo*, which was replaceable with Raf *in vitro*, were identified as fundamental components sufficient for mimicking *MLL*-fusion-mediated leukemogenesis. These findings suggest that the molecular crosstalk between aberrant expression of *Hox* molecule(s) and activated Raf may have a key role in the *MLL*-fusion-mediated-leukemogenesis, and may thus help develop the novel molecularly targeted therapy against *MLL*-related leukemia.**
Leukemia (2009) **23**, 2197–2209; doi:10.1038/leu.2009.177; published online 27 August 2009
Keywords: MLL; Ras; MAP kinase; leukemogenesis

Introduction

Multistep oncogenesis has been suggested in malignancy by the observation of more than two heterogeneous genetic and/or epigenetic lesions.[1] In leukemogenesis, recurring chromosomal translocations are frequently found in hematological malignancies, which sometimes coincide with subtle but critical genetic mutations leading to functional aberration.[2–4] Earlier studies showed that many of the translocation target genes are transcription factors involved in hematopoietic differentiation and/or self-renewal, whereas coincident mutations often occur on the genes involved in cell proliferation.[4] These results lead to a hypothetical model of leukemogenesis in which these two kinds of genetic alterations may cooperate to induce acute leukemia. This concept has been recently exemplified in experimental models using combinations of fusion genes, including *mixed-lineage leukemia* (*MLL*, also called *ALL1* or *HRX*) or *AML1* fusion genes, and other coincident genetic mutations.[5–9]

MLL is a proto-oncogene that is rearranged in human acute leukemia with chromosome 11 band q23 (11q23) translocation,[10,11] encoding a histone methyltransferase that assembles in a chromatin-modifying supercomplex.[12] Meanwhile, *MLL* fusion gene leads to leukemogenesis through several *HOX* genes directly transactivated by *MLL* fusion protein itself.[4,11,13,14] It is noteworthy that most of the genetically engineered mice carrying the *MLL* fusion developed hematological malignancy after a long latency, suggesting that secondary genotoxic stress is required to develop overt acute leukemia.[15–18] An earlier study presented direct evidence that *MLL* fusion proteins induced myeloproliferative disease (MPD) with a long latency, and caused acute leukemia with a short latency together with a coincident mutation of *FMS-like tyrosine kinase 3* (*FLT3*).[6]

Recent studies revealed that genetic alterations, including *FLT3*, *NRAS* (neuroblastoma RAS viral (v-ras) oncogene homolog) and *KRAS* (v-Ki-ras2 Kirsten rat sarcoma viral oncogene homolog), are frequently accompanied by 11q23 translocation.[19,20] *FLT3* is a receptor tyrosine kinase involved in leukemogenesis and normal hematopoiesis.[21] The mutations of *FLT3* are mainly classified into length mutations such as internal tandem duplication (ITD) of the juxtamembrane domain, and point mutations within the activation loop of the second tyrosine kinase domain (TKD).[21] Interestingly, *FLT3*-TKD, as well as overexpression of the wild type of FLT3, is found to be frequently associated with infant acute lymphoid leukemia (ALL), with rearrangements of *MLL*.[19,22] Both types of *FLT3* mutations result in a constitutive activation of *FLT3* kinase activity, followed by activation of signaling pathways, including signal transducer and activator of transcription 5 (STAT5) and Ras/Raf/mitogen-activated protein (MAP) kinase.[23,24] Both STAT5 and Ras/Raf/MAP kinase (MAPK) are involved in cellular

Correspondence: Dr T Nosaka, Department of Microbiology and Molecular Genetics, Mie University Graduate School of Medicine, 2-174 Edobashi, Tsu, Mie 514-8507, Japan.
E-mail: nosaka@doc.medic.mie-u.ac.jp
Received 1 October 2008; revised 17 July 2009; accepted 21 July 2009; published online 27 August 2009

proliferation, survival and differentiation.[25,26] Constitutively active mutants of Ras induce oncogenic transformation through activation of the MAPK cascade.[26] However, little has so far been elucidated regarding the molecular mechanism of collaboration in leukemogenesis.

To further clarify the molecular mechanism of *MLL*-fusion-mediated leukemogenesis, we focused on signal transduction associated with malignant transformation that collaborates with *MLL* fusion protein *in vitro*, and highlighted the contrastive roles of STAT5 and MAPK in leukemogenesis. Interestingly, comparative analyses suggested synergistic collaboration with activated Ras in *MLL*-fusion-mediated leukemogenesis, and also activation of Raf in malignant transformation *in vitro*, but not with STAT5 activation *in vivo* and *in vitro*. Thus, the activation of Ras/Raf/MAPK cascade may have an important role in multistep leukemogenesis with 11q23 translocations.

Materials and methods

Construction of the plasmids and retrovirus production

Fragments of murine constitutively active mutants of STAT5A (#2[27] and 1*6[28]) fused with a FLAG tag at the C-terminus, a coding region of human *NRAS*^{G12V} and *MLL-eleven nineteen leukemia* (*ENL*) short form[6] were inserted upstream of the internal ribosomal entry site (IRES)-enhanced green fluorescent protein (EGFP) cassette of pMYs-IRES-EGFP.[29] Fragments of coding regions of a wild type of *NRAS* and *NRAS*^{G12V} were inserted into pMXs-puro.[29] A fragment of murine *Hoxa9*[30] (a kind gift from Dr G Sauvageau) was inserted into pMXs-IRES-EGFP.[29] A fragment of a dominant negative mutant (dn) of STAT5A[23] was inserted upstream of the IRES-Kusabira-Orange (KO)[31] cassette of pMXs-IRES-KO, in which the EGFP cassette in pMXs-IRES-EGFP[29] was replaced with the KO cassette of phKO1-S1 (MBL, Nagoya, Japan). pMXs-neo-*MLL-SEPT6*,[6] pMY-FLT3-ITD-IRES-EGFP,[6] pMY-FLT3^{D835V}-IRES-EGFP[6] and pBabe-puro-Δ*Raf*-estrogen receptor (ER)[28] were described earlier. Retroviruses were harvested 48 h after transfection with each retroviral construct into PlatE cells[29] in which appropriate expression of the transgenes was confirmed by western blot analysis, as described earlier.[6]

Cells

An *MLL-SEPT6*-immortalized murine myelomonocytic cell line, HF6, was established through colony-replating assays using retroviral transduction with pMXs-neo-*MLL-SEPT6* as described earlier.[6] A *Hoxa9*-immortalized murine myelomonocytic cell line, A9G, was established through infection with retroviruses harboring *Hoxa9* in pMXs/IRES-EGFP[29] as reported earlier.[32] The HF6,[6] A9G and murine pro-B Ba/F3[28] cells were cultured in the presence of interleukin-3 (IL-3) (R&D Systems, Minneapolis, MN, USA). HF6 cells transduced with *FLT3* mutants were cultured in the same medium, except for the absence of IL-3. The expression levels of *FLT3* in these cells were evaluated using a phycoerythrin (PE)-conjugated anti-CD135 antibody, or an anti-mouse immunoglobulin G1,κ, as the isotype-matched control (BD Biosciences, San Diego, CA, USA) using fluorescence-activated cell sorting (FACS) Calibur (BD Biosciences) as described earlier.[33]

Immunoprecipitation and western blot analysis

Fifty million parental and additionally transduced HF6 cells, or 10 million parental and transduced Ba/F3 cells, were harvested in the lysis buffer, and the lysates were either suspended with 1 × sodium dodecyl sulfate sample buffer after immunoprecipitation using polyclonal anti-STAT5A antibody (L-20) (Santa Cruz Biotechnology, Santa Cruz, CA, USA) or directly mixed with an equal volume of 2 × sodium dodecyl sulfate sample buffer and then boiled, as described earlier.[25] In some experiments, the parental HF6 cells had been deprived of IL-3 8 h before harvest. Western blot analysis of each sample was performed using the polyclonal anti-STAT5A (L-20), monoclonal anti-phosphotyrosine (4G10) (Upstate Biotechnology, Lake Placid, NY, USA), polyclonal anti-extracellular signal-related kinase (ERK)1/2, monoclonal anti-phospho-ERK1/2 (E10) (Cell Signaling Technology, Danvers, MA, USA), monoclonal anti-α-tubulin (Sigma-Aldrich, St Louis, MO, USA), monoclonal anti-FLAG (M2), polyclonal anti-ERα (MC-20) and monoclonal anti-N-Ras (F155) (Santa Cruz Biotechnology) antibodies to probe membranes, as described earlier.[25]

Evaluation of cellular effects by inhibition of signal transduction in vitro

The response to the drug was evaluated as described earlier.[23] In brief, HF6 cells expressing the *FLT3* mutants (3×10^5) were infected with retroviruses harboring or not harboring the dnSTAT5A in pMXs-IRES-KO in the presence of polybrene, as described earlier.[6] Viable cell numbers were counted with standard Trypan blue staining, and the expression of the dnSTAT5A was monitored by assessment of KO positivity using the FL2 channel on the FACS Calibur, daily after infection. At 48 h after infection, to evaluate the status of phosphorylated STAT5, half a million of these cells were fixed with fixation buffer, permeablized with Perm Buffer III and analyzed with an Alexa Fluor 647-conjugated anti-phospho-STAT5 (Y694) (all from BD Biosciences) antibody, or the anti-mouse immunoglobulin G1,κ, as the isotype-matched control antibody, using the FL4 channel on the FACS Calibur, according to the manufacturer's recommendation. As controls, the parental HF6 cells with and without IL-3 stimulation after deprivation of IL-3 for 8 h were used. Meanwhile, these HF6 cells (1×10^4) were cultured for 72 h in 24-well plates in the presence of various concentrations of a MAPK kinase (MEK) inhibitor, U0126, or a PI3 kinase inhibitor, LY294002 (Calbiochem-Novabiochem, San Diego, CA, USA) and each vehicle control (ethanol for U0126 and dimethyl sulfoxide for LY294002). Viable cell numbers were counted with standard Trypan blue staining after each treatment, followed by calculation of the 50% inhibitory concentration (IC50) of each drug using a logistic regression model. To evaluate the inhibitory effect of U0126 on ERK1/2, five million of the cells were treated for 2 h, harvested and analyzed with the anti-ERK1/2 or the anti phospho-ERK1/2 antibody after western blotting.

Myeloid transformation assays in vitro

In a series of transformation assays, the acquisition of IL-3-independent proliferation was examined in IL-3-dependent cells. HF6 and Ba/F3 cells were infected with retroviruses harboring *NRAS*, *NRAS*^{G12V} or mock in pMXs-puro; Δ*Raf*-ER or mock in pBabe puro; and STAT5A1*6, STAT5A#2 or none (only GFP) in pMYs-IRES-EGFP, respectively, in the presence of polybrene, as described earlier.[6] A9G cells were also retrovirally transduced with *NRAS*, *NRAS*^{G12V} Δ*Raf*-ER or each mock in the same way. For puromycin selection, the transduced cells were cultured with 1 μg/ml of puromycin 24–96 h after infection, followed by propagation for 5 days in the absence of puromycin.

Next, 1×10^5 puromycin-resistant cells transduced with *NRAS*, *NRAS*^{G12V} or mock were cultured in 24-well plates in the absence of IL-3, whereas those transduced with Δ*Raf*-ER or mock were cultured under the same condition, except for the presence of 1 μM of 4-hydroxy-tamoxifen or a vehicle control (ethanol). The cells transduced with STAT5A1*6, STAT5#2 or none were purified on the basis of the expression of GFP using a FACS Aria (BD Biosciences) 36 h after infection. Immediately, these purified cells (1×10^4) were cultured in 96-well plates in the absence of IL-3, to avoid excessive signals caused by STAT5A#2 or 1*6 in the presence of IL-3, which led to cell death as described earlier.[25] Viable cell numbers were counted periodically after standard Trypan blue staining.

Leukemogenesis assays in vivo

Leukemogenesis assays *in vivo* using C57BL/6 mice produced by a combination of two kinds of transgenes were performed with lethal conditioning using lethally (9.5 Gy) irradiated recipients, or with sublethal conditioning using sublethally (5.25 Gy) irradiated recipients receiving no radioprotective bone marrow (BM) cells, as described earlier[6] (Supplementary Figure 1). In brief, hematopoietic progenitors were harvested from 6- to 10-week-old Ly-5.1 C57BL/6 mice 4 days after intraperitoneal administration of 150 mg/kg 5-fluorouracil, and cultured overnight in alpha minimal essential medium supplemented with 20% fetal calf serum and 50 ng/ml each of mouse stem cell factor, human IL-6, human FLT3-ligand (R&D Systems) and human thrombopoietin (Kirin Brewery, Takasaki, Japan). The prestimulated cells were infected with several combinations of the retroviruses for 60 h in the α minimal essential medium supplemented with the same fetal calf serum and cytokines using RetroNectin (Takara Bio Inc., Otsu, Japan) according to the manufacturer's recommendations, followed by intravenous injection of 10^5 of the cells into Ly-5.2 mice together with either a radioprotective dose (2×10^5) of Ly-5.2 cells under lethal conditioning or none under sublethal conditioning. Morbid mice and their tissue samples were analyzed, and immunophenotyping of BM, splenic and thymic cells was performed using the FACS Calibur, as described earlier.[33] The hematopoietic neoplasms were diagnosed mainly on the basis of morphology as described earlier.[6] The probabilities of murine overall survival were estimated using Kaplan–Meier method and compared using the log-rank test. All animal studies were performed in accordance with the guidelines of the Animal Care Committees of the Institute of Medical Science, the University of Tokyo and the Mie University.

Southern blot analysis

Genomic DNA was extracted from spleens, digested with *Nhe*I or *Bam*HI for detecting proviral integration and clonality, respectively, and analyzed with the Neo or puro probe (Supplementary Figure 1) as described earlier.[34]

Reverse transcriptase-polymerase chain reaction (PCR)

Total RNA was extracted from cell lines, spleen or BM, and reverse transcribed to complementary DNA as described earlier.[6] The conditions, reagents for reverse transcriptase-PCR and the primers specific for β_2*microglobulin* (β_2*MG*), *Hoxa9* and *MLL-SEPT6* have been described earlier,[6] except that PCR amplification for *MLL-SEPT6* transcripts was sometimes run for 35 cycles. To detect the transcript of *NRAS*^{G12V}, PCR amplification was run for 21 cycles using the following primers: *NRAS-S*, 5′-GTGGTTATAGATGGTGAAACCTGTT-3′ and *NRAS-AS*, 5′-GACCATAGGTACATCTTCAGAGTCCT-3′.

Results

MLL-SEPT6 *cooperates with both types of* FLT3 *mutations through different modes of signal transduction*

To clarify the molecular mechanism of cooperation between *MLL* fusion proteins and *FLT3* mutants, signaling pathways of *FLT3*-ITD and *FLT3*-TKD that cooperate with *MLL-SEPT6* were examined using the IL-3-dependent *MLL-SEPT6*-immortalized cell line, HF6.[6] Earlier, STAT5 and MAPK ERK1/2 had been found to be activated downstream of *FLT3* mutants in factor-dependent cell lines.[23,24] Therefore, the activation of these molecules was first examined using parental HF6 and transformed HF6 cells expressing FLT3-*ITD* (HF6^{ITD}) or *FLT3*^{D835V} (HF6^{D835V}) described earlier.[6] Nearly equal levels of expression of the *FLT3* mutants in the transformed HF6 cells were confirmed (Figure 1a). A western blot analysis after immunoprecipitation of the lysates from these cells revealed constitutive phosphorylation of STAT5A in HF6 cells expressing the FLT3 mutants in the absence of IL-3, but little in the parental HF6 cells that had been deprived of IL-3 (Figure 1b). In addition, a western blot analysis of the same lysates also revealed constitutive phosphorylation of ERK1/2 in those cells expressing the *FLT3* mutants, but little in the parental HF6 cells that had been deprived of IL-3 (Figure 1b).

Next, to determine whether STAT5 and/or MAPK were important in the transformation of HF6 cells expressing *FLT3* mutants, each signaling pathway was inhibited using dnSTAT5A or MEK inhibitor U0126. After retroviral transduction with the dnSTAT5A, the proliferation of HF6^{ITD} cells expressing dnSTAT5A was suppressed more efficiently than that of HF6^{D835V} cells expressing dnSTAT5A (Figure 2a). KO-positive cells expressing dnSTAT5A showed higher levels of phosphorylated STAT5 than KO-negative cells (Figure 2b). This finding is consistent with the earlier report showing that the dnSTAT5A exerts its effect on endogenous STAT5A and 5B with persistent phosphorylation of the dnSTAT5A itself.[35] In contrast, U0126 retarded the proliferation of the HF6^{D835V} cells more effectively than the HF6^{ITD} cells (Figure 2c, each IC50 is 0.67 ± 0.35 μM for HF6^{D835V} and 6.09 ± 0.90 μM for HF6^{ITD} in the absence of IL-3). Indeed, U0126 inhibited phosphorylation of ERK1/2 in the HF6^{ITD} and HF6^{D835V} cells in a semidose-dependent manner (Figure 2d). In addition, another important signaling pathway downstream of *FLT3*, through PI3 kinase, was inhibited using LY294002. LY294002 also retarded the growth of the HF6^{D835V} and HF6^{ITD} cells in a dose-dependent manner, but there was no remarkable difference between both types of HF6 cells (Supplementary Figure 2, each IC50 is 4.18 ± 0.55 μM for HF6^{D835V} and 8.12 ± 1.54 μM for HF6^{ITD} in the absence of IL-3).

Taken together, these results *in vitro* suggested that the activation of MAPK was more critical for transformation by *FLT3*-TKD than by *FLT3*-ITD in HF6 cells, whereas activation of STAT5 was more critical for transformation by *FLT3*-ITD than by *FLT3*-TKD.

Activation of Ras-MAPK cascade enables HF6 cells to grow without IL-3 through cooperation between Hoxa9 *and Raf*

We further examined whether direct activation of either STAT5 or MAPK cascade is sufficient to confer factor-independent

growth on HF6 cells. Although the constitutively active mutants of STAT5A, the relatively stronger mutant STAT5A1*6 and weaker mutant STAT5A#2, enabled Ba/F3 cells (Ba/F3^{1*6}, Ba/F3$^{\#}$) to grow without IL-3 as reported earlier,[25,27,28] both failed to confer factor-independent growth on HF6 cells with limited elongation of survival time without IL-3 (Figures 3a and c). In contrast, the oncogenic *NRAS* mutant, *NRAS*^{G12V}, which had been detected in a case of *AML* with *MLL-SEPT6*,[20] enabled HF6 cells (HF6^{G12V}) to grow without IL-3, while it conferred no factor-independent growth on Ba/F3 with limited elongation of survival time without IL-3 (Figures 3b and c). In addition, Raf-1, a signal molecule downstream of Ras in Ras-MAPK cascades associated with malignant transformation, was tested with an activation-inducible system using Δ*Raf*-ER, consisting of the catalytic domain of human RAF-1 (ΔRaf) and the hormone-binding domain of the ER (Figure 3d), as described earlier.[28]

Unlike transduced Ba/F3 (Ba/F3$^{\Delta Raf\text{-}ER}$) cells, transduced HF6 (HF6$^{\Delta Raf\text{-}ER}$) cells grew without IL-3 only in the presence of 4-hydroxy-tamoxifen (Figure 3e). In these HF6$^{\Delta Raf-ER}$ cells treated with 4-hydroxy-tamoxifen, STAT5A was not found to be secondarily activated by induction of activation of Raf/MAPK cascade in the absence of IL-3, whereas it was found to be weakly activated by stimulation with IL-3 for 15 min (data not shown).

Furthermore, we examined whether *Hoxa9*, which is one of the well-known target genes of *MLL* fusion proteins,[10,11,13,14] is involved in cooperation between *MLL* fusion protein and Ras/Raf/MAPK cascade. In the myeloid transformation assays, the murine BM progenitors immortalized by *Hoxa9* in the presence of IL-3 (named A9G) proliferated without IL-3 after retroviral transduction of *NRAS*^{G12V} (Figure 3b). In the inducible transformation system using Δ*Raf*-ER, transduced A9G

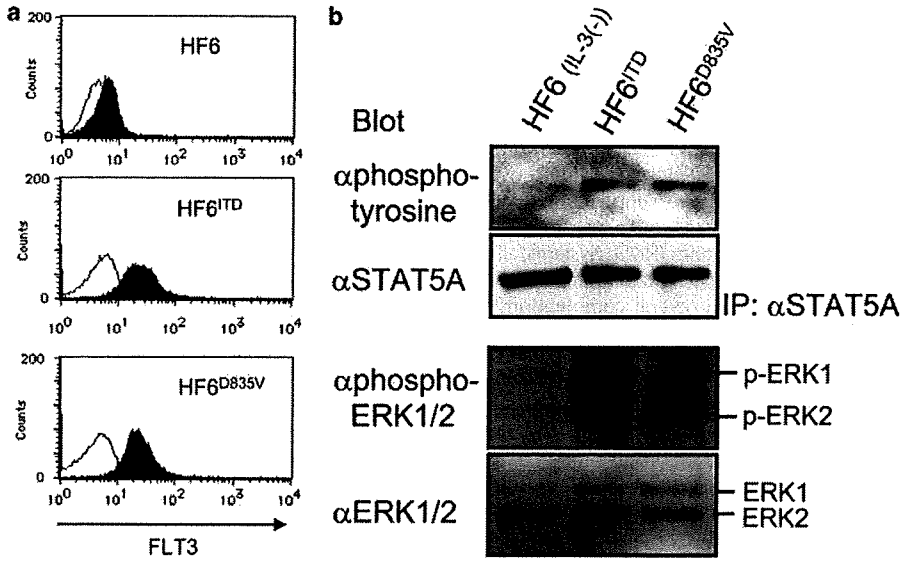

Figure 1 Characterization of signal transduction in the HF6 cells transformed by *FMS-like receptor tyrosine kinase 3* (*FLT3*) mutants. (**a**) Expression of each *FLT3* mutant in HF6 and their transformed cells. The shadow profiles and black lines represent fluorescence-activated cell sorting (FACS) staining obtained using the antibody specific to *FLT3* and its isotype control antibody, respectively. (**b**) Western blot analyses of proteins extracted from HF6 and their transformed cells after immunoprecipitation using the anti-signal transducer and activator of transcription 5A (STAT5A) antibody (upper two panels), and of the whole lysates (lower two panels). The parental HF6 cells had been deprived of interleukin-3 (IL-3) 8 h before harvest. The blot of the immunoprecipitated samples was probed with the anti-STAT5A antibody (upper bottom panel), followed by reprobe with 4G10 (the anti-phosphotyrosine antibody) (upper top panel). The blot of the whole lysates was probed with the anti-extracellular signal-related kinase (ERK)1/2 antibody (lower bottom panel), followed by reprobe with the anti-phospho-ERK1/2 antibody (lower top panel).

Figure 2 Differential effects of inhibition of cellular signal transduction on the HF6 cells transformed by *FMS-like receptor tyrosine kinase 3* (*FLT3*) mutants. (**a**) Effect of the retroviral transduction with the dominant negative mutant of signal transducer and activator of transcription 5A (dnSTAT5A) in pMXs-internal ribosomal entry site (IRES)-Kusabira-Orange (KO) on the transformed and parental HF6 cells. Viable cell numbers and KO expression were monitored daily after the transduction, and the averages of ratios of each KO-positive cell number at days 1, 2, 3 and 4 to that at day 1 are shown with s.d. (bars). (**b**) Intracellular flow cytometric analyses of phospho-STAT5 (Y694) on the transformed and parental HF6 cells transduced with dnSTAT5A in pMXs-IRES-KO. The density plots show expression of each intracellular antigen labeled with the Alexa Fluor 647-conjugated anti-phospho-STAT5 (Y694) (upper eight panels) or its isotype control (lower two panels) antibody versus expression of KO. As negative controls, nontransduced and mock-transduced HF6 cells were used, respectively (lower two panels using the isotype control antibody). As references, nontransduced HF6 cells were deprived of interleukin-3 (IL-3) for 8 h (HF6 (IL-3(−))), or stimulated with IL-3 for 15 min after the same deprivation (HF6 (IL-3(+))), and then used (lower two panels using the anti-phospho-STAT5 antibody). KO and Alexa Fluor 647 were detected using the FL2 and FL4 channels of the fluorescence-activated cell sorting (FACS) Calibur, respectively. (**c**) Effect of the various concentrations of mitogen-activated protein kinase (MAPK) kinase (MEK) inhibitor, U0126, on the transformed and the parental HF6 cells. The averages with s.d. (bars) of ratios of viable cell numbers in the presence of each concentration of U0126 to those in the absence of U0126 are shown. (**d**) Western blot analyses of the whole lysates extracted from the transformed HF6 cells treated with U0126. Both groups of transformed HF6 cells were treated with various concentrations (shown above each upper panel) of U0126 for 2 h and then harvested. Both blots were probed with the anti-phospho-extracellular signal-related kinase (ERK)1/2 antibody (each top panel), followed by reprobe with the anti-ERK1/2 antibody (each bottom panel).

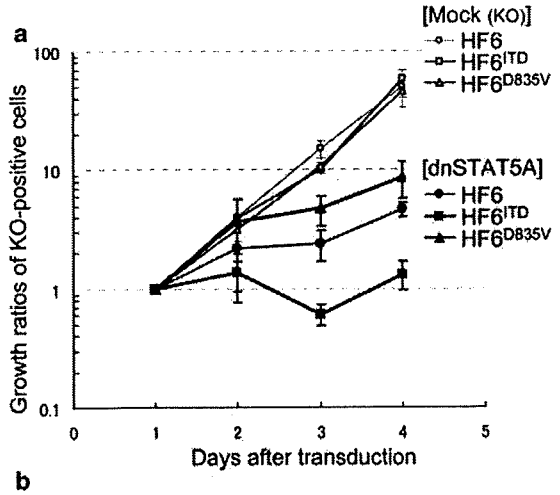
a
[Mock (KO)]
HF6
HF6ITD
HF6D835V
[dnSTAT5A]
HF6
HF6ITD
HF6D835V
Growth ratios of KO-positive cells
Days after transduction

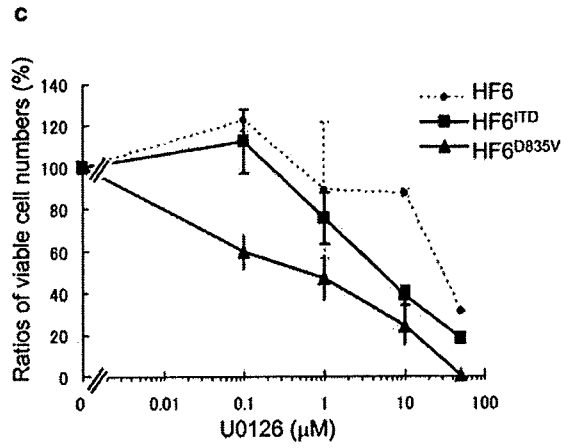
c
HF6
HF6ITD
HF6D835V
Ratios of viable cell numbers (%)
U0126 (μM)

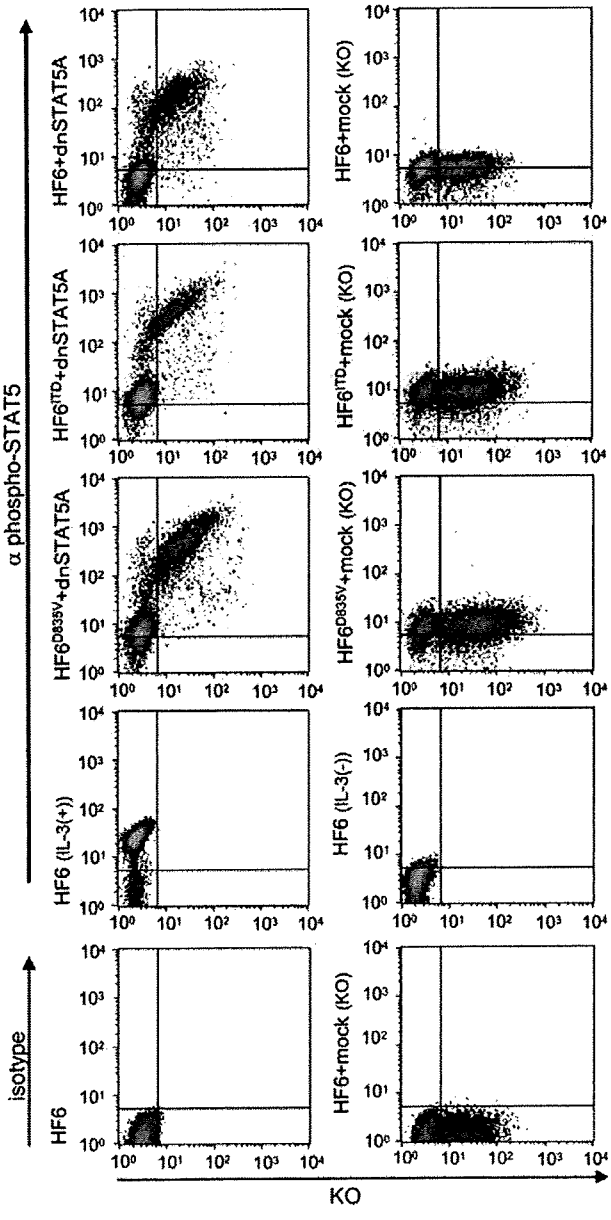
b
α phospho-STAT5
HF6+dnSTAT5A
HF6+mock (KO)
HF6ITD+dnSTAT5A
HF6ITD+mock (KO)
HF6D835V+dnSTAT5A
HF6D835V+mock (KO)
HF6 (IL-3(+))
HF6 (IL-3(-))
isotype
HF6
HF6+mock (KO)
KO

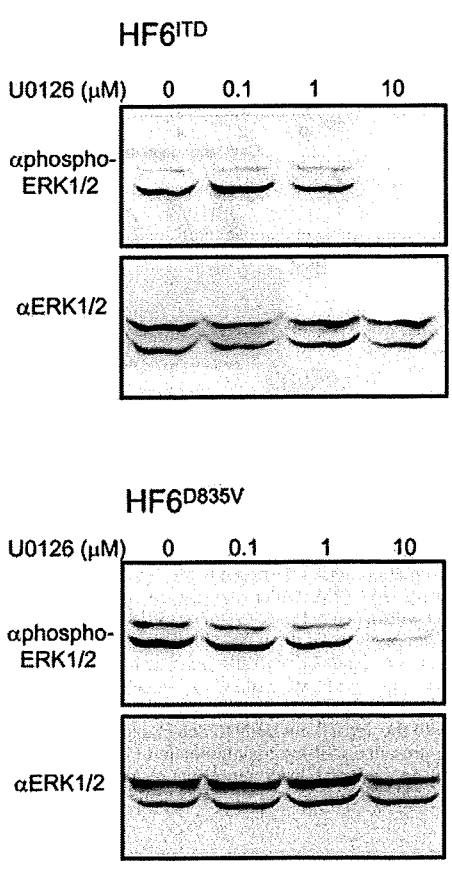
d
HF6ITD
U0126 (μM) 0 0.1 1 10
αphospho-ERK1/2
αERK1/2
HF6D835V
U0126 (μM) 0 0.1 1 10
αphospho-ERK1/2
αERK1/2

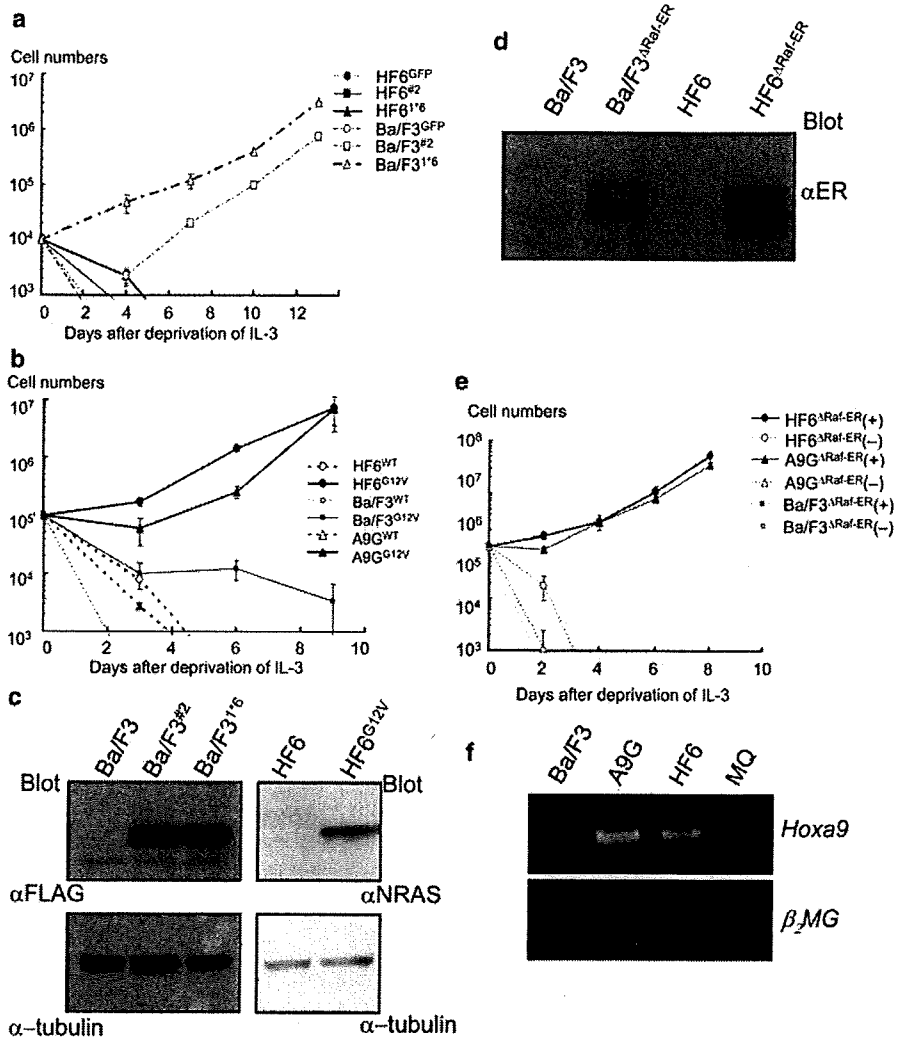

Figure 3 Transformation of the HF6 and A9G cells induced by direct activation of Ras/Raf/mitogen-activated protein kinase (MAPK) pathway. (**a**) Transformation assays of the HF6 and Ba/F3 cells expressing constitutively active forms of signal transducer and activator of transcription 5A (STAT5A) (#2 and 1*6). Green fluorescent protein (GFP) was used as a control. (**b**) Transformation assays of the HF6, A9G and Ba/F3 cells expressing wild-type (WT) *NRAS* or $NRAS^{G12V}$ (G12V). The averages of the number of viable cells with s.d. (bars) are shown in (**a**) and (**b**). (**c**, **d**) Western blot analyses of the whole lysates extracted from the transduced cells (see legends to panels (a) and (b)) in the absence of interleukin-3 (IL-3). (**c**) HF6 and Ba/F3 cells transduced with an inducible form of Raf (Δ*Raf*-estrogen receptor (ER)) (**d**) and their parental cells (**c**, **d**). The blot was probed with the anti-FLAG antibody to detect expression of ectopically expressed STAT5A mutants (upper left panel), or probed with the anti-*NRAS* antibody (upper right panel), followed by reprobe with the anti-α-tubulin antibody as internal control (lower panels) (**c**). The blot was also probed with the anti-ER antibody to detect expression of Δ*Raf*-ER (**d**). (**e**) Transformation assays of the HF6, A9G and Ba/F3 cells expressing Δ*Raf*-ER in the presence of 4-hydroxy-tamoxifen (4-OHT) (+) or vehicle control (–). The averages of the number of viable cells with s.d. (bars) are shown. (**f**) Analysis of *Hoxa9* transcripts in A9G cells using reverse transcriptase-PCR. Ba/F3 and HF6 cells were used as negative and positive controls, respectively.

Figure 4 Leukemogenesis induced by *mixed-lineage-leukemia* (*MLL*)-septin 6 (*SEPT6*) with $NRAS^{G12V}$ synergistically, but not with signal transducer and activator of transcription 5A (STAT5A)#2, *in vivo* under lethal conditioning. (**a**) Survival curves of mice transplanted with *MLL-SEPT6* and $NRAS^{G12V}$ (MS6/G12V; $n=6$), MS6 and *STAT5A*#2 (MS6/#2; $n=6$), MS6/GFP ($n=6$), neo/G12V ($n=6$), neo/#2 ($n=3$) and neo/GFP ($n=3$). (**b**) Representative macroscopic images of spleens obtained from each group of mice shown in (**a**). Scale bar 1 cm. (**c**, **d**) Representative histopathological analysis of morbid mice transplanted with MS6/#2, MS6/G12V (**c**, **d**), neo/G12V, and neo/#2 (**d**). Bone marrow (BM) cells (**c**) and paraffin sections of spleen (**d**) were stained with Wright-Giemsa and hematoxylin and eosin (H&E), respectively. Original magnification, × 200 (**c**) and × 40 (**d**); scale bars, 30 μm (c) and 200 μm (**d**). (**e**, **f**) Immunophenotype of BM or splenic (Sp) cells obtained from representative morbid mice transplanted with MS6/#2 (**e**, left panels), MS6/G12V (**e**, right panels), neo/G12V (**f**, left panels) and neo/#2 (**f**, right panels). The dot plots show each surface antigen labeled with a corresponding monoclonal antibody versus expression of GFP. Ly5.1, Gr-1, CD11b, Ter119, and c-Kit were labeled with phycoerythrin (PE)-conjugated and allophycocyanin (APC)-conjugated monoclonal antibodies, respectively. (**g**) Southern blot analysis to detect clonality (left panel) and proviral integration (right panel). Genomic DNA extracted from BM cells obtained from representative mice transplanted with MS6/G12V (lanes 4, 5, 9 and 10), MS6/GFP (lanes 2, 3, 7 and 8) and neo/GFP (5 months after transplantation; lanes 1 and 6) was digested with *Bam*HI (lanes 1–5) and *Nhe*I (lanes 6–10), respectively, and hybridized with the Neo probe. Oligoclonal bands of proviral integration and single bands of the proviral DNA are indicated by arrows and arrowheads, respectively.

(A9G$^{\Delta Raf-ER}$) cells grew without IL-3 only in the presence of 4-hydroxy-tamoxifen (Figure 3e). Expression level of *Hoxa9* in A9G cells was shown in comparison with those in Ba/F3 and HF6 (negative and positive controls, respectively) cells by reverse transcriptase-PCR (Figure 3f).

Taken together, these results *in vitro* suggested the essential role of activation of the Ras/Raf/MAPK cascade together with *Hoxa9* upregulated by *MLL* fusion proteins in the transformation of the cells expressing *MLL* fusion protein.

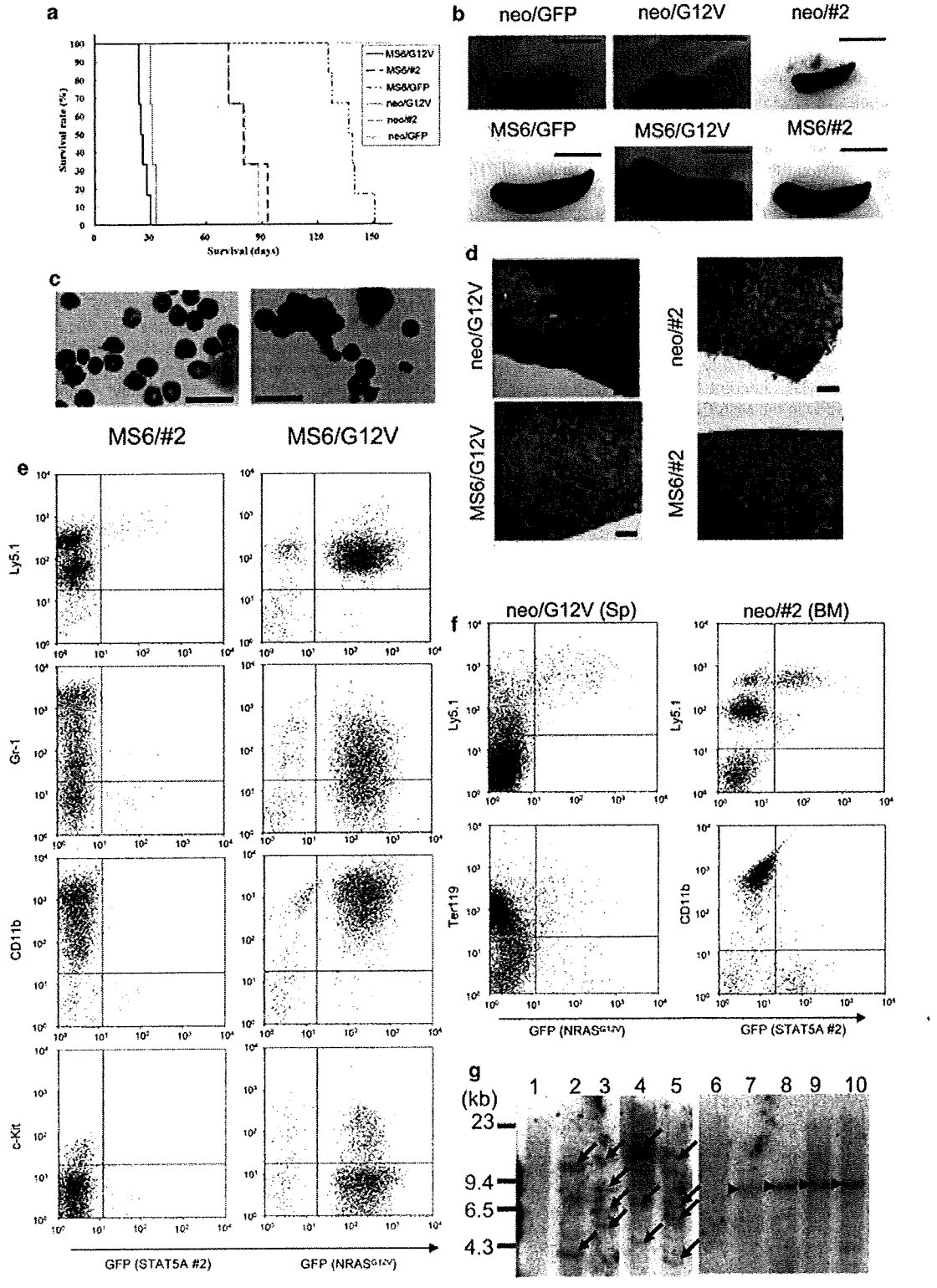

MLL *fusion proteins and oncogenic* NRAS *cooperate to induce acute leukemia, at least partly through aberrant expression of* Hoxa9

The findings on the transformation of HF6 cells *in vitro* led to the hypothesis that *MLL* fusion proteins might cooperate with activation of Ras to induce *AML in vivo*. To test this hypothesis, the oncogenic potential of $NRAS^{G12V}$ (G12V) or STAT5A#2 (#2) to cooperate with *MLL-SEPT6* (MS6) or *MLL-ENL* short form was examined in the leukemogenesis assays *in vivo* (Supplementary Figure 1). STAT5A1*6 was not used owing to its too strong oncogenic potential *in vivo* as reported earlier.[36] The transduction efficiencies of $NRAS^{G12V}$, STAT5A#2 and *MLL-ENL* were 30–50, 20–40 and 5–10%, respectively, as determined by GFP expression (data not shown).

The mice receiving the BM cells transduced with *MLL-SEPT6* and $NRAS^{G12V}$ (MS6/G12V) died with significantly shorter latencies (26 ± 2.4 days; $P<0.05$, log-rank test) than the MS6/GFP mice that died of MPD (137 ± 9.0 days) as described earlier,[6] but, unexpectedly, the neo/G12V mice died as early as the MS6/G12V mice (31 ± 1.4 days) (Figure 4a, Table 1, and data not shown). The MS6/#2 mice died with significantly shorter latencies (82 ± 11 days; $P<0.05$, log-rank test) than the MS6/GFP mice, but as early as the neo/#2 mice (80 ± 8.0 days) (Figure 4a and Table 1). Notably, the phenotypes of the MS6/G12V mice were very different from those of the neo/G12V mice and from MPD in the MS6/GFP mice, whereas those of the MS6/#2 mice were rather similar to MPD in the MS6/GFP mice than those of the neo/#2 mice.

The morbid MS6/G12V mice showed hepatosplenomegaly with various ranges of leukocytosis, anemia and thrombocytopenia, whereas the morbid neo/G12V mice showed no hepatomegaly but mild splenomegaly, and severe pancytopenia (Figure 4b and Table 1). Histopathological analyses of the morbid MS6/G12V mice showed that immature myelomonocytic blasts accounted for more than 30% of BM cells, and severely infiltrated the spleen and the liver (Figures 4c and d, and data not shown). Immunophenotyping analyses of the BM cells also revealed that a majority of these cells expressed GFP, which indicated expression of $NRAS^{G12V}$, with high level of CD11b, intermediate level of Gr-1 (a myeloid differentiation marker also known as Ly-6G) and low level of c-Kit (CD117, the receptor of stem cell factor) (Figure 4e). In addition, Southern blot analysis of genomic DNAs derived from the spleens of the MS6/G12V mice showed oligoclonal bands of proviral integration (Figure 4g). These results indicated that the MS6/G12V mice developed *AML* similar to the mice receiving BM cells transduced with *MLL-SEPT6* and *FLT3*-ITD, as described earlier.[6] In contrast, the morbid neo/G12V mice showed extremely hypocellular marrows and extramedullary hematopoiesis in the spleen, where a majority of the cells did not express Ly5.1 (Figure 4f), with little expression of *Hoxa9* in comparison with the morbid MS6/G12V mice (Supplementary Figure 3a). Thus, this finding suggested that, in our leukemogenesis assays under lethal conditioning, *NRAS* might develop BM aplasia presumably due to engraftment failure. Meanwhile, the MS6/#2 mice died of MPD, showing myeloid hyperplasia consisting predominantly of mature granulocytic elements in the BM cells, where a very small population (1.0%) expressed STAT5A#2, with splenomegaly similar to the MS6/GFP mice (Figures 4b–d, and Table 1). The neo/#2 mice showed neither hepatosplenomegaly nor hematological abnormalities in the peripheral blood, but relative myeloid hyperplasia in the BM, where only a small population (9.4%) expressed STAT5A#2 (Figures 4b and f, data not shown and Table 1), thus implying that STAT5A#2 might induce lethal BM abnormality owing to paracrine expression of some cytokines as in the earlier report using STAT5A1*6.[36]

To generalize leukemogenic cooperation between *MLL* fusion proteins and oncogenic *NRAS* and avoid the early death caused by transduction of $NRAS^{G12V}$, the BM cells transduced with *MLL-ENL* and/or oncogenic *NRAS* were also transplanted into recipient mice under sublethal conditioning. The *MLL-ENL* short form was used for leukemogenesis assays under sublethal conditioning with oncogenic *NRAS* ($NRAS^{G12V}$), in which retroviral vectors were exchanged, so that the expression of GFP indicated that of *MLL-ENL* (Supplementary Figure 1). These leukemogenesis assays under sublethal conditioning confirmed that the combination of *MLL-ENL* and $NRAS^{G12V}$ reproduced *AML*, and that *MLL-ENL* (and puro) induced the phenotype of MPD (Figures 5a, b and d, and Table 1). Meanwhile, $NRAS^{G12V}$

Table 1 Characteristics of the morbid mice transplanted with hematopoietic progenitors transduced with *MLL* fusion genes or *Hoxa9*, and/or either $NRAS^{G12V}$ or STAT5A #2

Mouse	*Latency (days)*	*Liver (g)*	*Spleen (g)*	*Thymus (g)*	*WBC (per μl)*	*Hb (g per 100 ml)*	*Plt (× 10^4 per μl)*
Lethal conditioning							
MS6/G12V ($n=6$)	26 ± 2.4	1.60 ± 0.35	0.31 ± 0.07	0.020 ± 0.012	74 600 ± 62 900	4.2 ± 1.0	4.0 ± 3.9
MS6/#2 ($n=3$)[a]	82 ± 11	0.98 ± 0.43	0.32 ± 0.03	0.019 ± 0.006	73 100	5.3	4.4
MS6/GFP ($n=6$)	137 ± 9.0	1.54 ± 0.69	0.26 ± 0.09	0.037 ± 0.005	309 000 ± 263 000	7.0 ± 6.6	8.0 ± 5.7
neo/G12V ($n=6$)	31 ± 1.4	1.04 ± 0.25	0.25 ± 0.08	0.030 ± 0.030	4600 ± 1800	2.5 ± 0.3	0.5 ± 0.4
neo/#2 ($n=3$)[a]	80 ± 8.0	0.66 ± 0.16	0.08 ± 0.06	0.011 ± 0.001	9800	18.8	58.2
neo/GFP ($n=3$)	NA	1.36 ± 0.11	0.09 ± 0.01	0.051 ± 0.010	12 000 ± 4700	14.7 ± 0.6	81 ± 13
A9/G12V ($n=4$)	28 ± 7.5	1.93 ± 0.56	0.44 ± 0.16	0.033 ± 0.030	76 300 ± 56 700	4.5 ± 2.7	1.0 ± 0.6
A9/GFP ($n=6$)	NA	NT	NT	NT	21 200 ± 5400	17.3 ± 2.4	66 ± 4.7
puro/GFP ($n=3$)	NA	1.48 ± 0.21	0.06 ± 0.01	0.049 ± 0.022	12 000 ± 3400	13.6 ± 1.5	81 ± 19
Sublethal conditioning							
MEs/G12V ($n=10$)	21 ± 3.9	2.56 ± 0.45	0.51 ± 0.10	0.043 ± 0.020	164 000 ± 131 000	7.2 ± 2.5	11 ± 4.5
MEs/puro ($n=5$)	89 ± 11	1.89 ± 0.58	0.44 ± 0.11	0.043 ± 0.006	99 000 ± 53 000	7.4 ± 2.9	9.1 ± 3.1
GFP/G12V ($n=5$)[b]	89 ± 10	0.90 ± 0.31	0.06 ± 0.03	0.63 ± 0.35	22 000 ± 1000	13.6 ± 1.7	97
GFP/puro ($n=3$)	NA	NT	NT	NT	NT	NT	NT

Abbreviations: GFP, green fluorescent protein; Hb, hemoglobin; MEs, *MLL-ENL* short form; NA, not applicable; NT, not tested; Plt, platelet; WBC, white blood cell.
Averages with s.d. are shown.
[a]Blood cell counts of only one morbid mouse were performed.
[b]One mouse developing acute leukemia and thymoma was excluded, owing to the remarkably increased number of WBCs and hepatosplenomegaly. The platelet count of only one morbid mouse was determined.

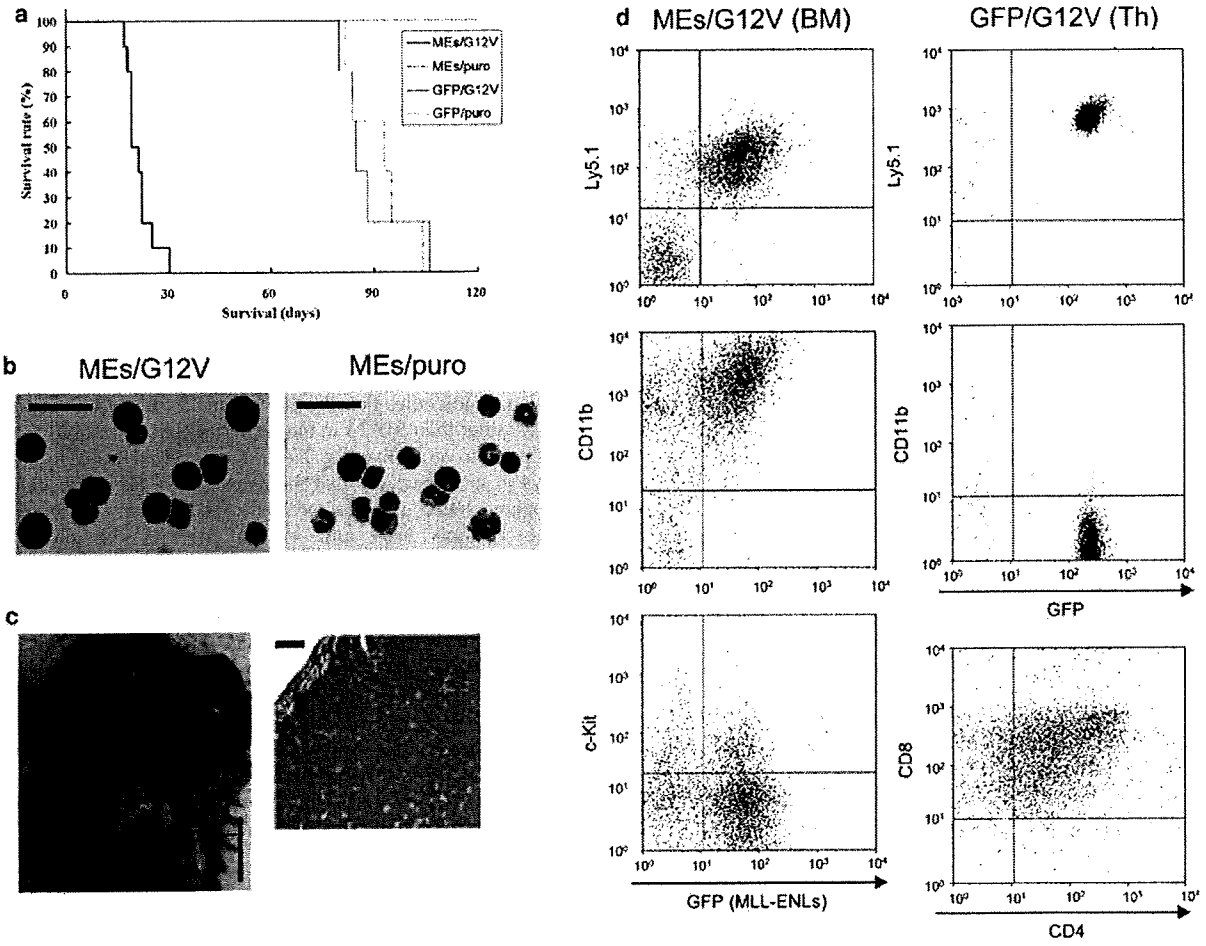

Figure 5 Leukemogenesis assays under sublethal conditioning using *mixed-lineage-leukemia/eleven nineteen leukemia* (*MLL-ENL*) and *NRAS*^{G12V}. (**a**) Survival curves of mice transplanted with a short form of *MLL-ENL* (MEs) and *NRAS*^{G12V} (MEs/G12V) ($n=10$), MEs/puro ($n=5$), GFP/G12V ($n=5$) and green fluorescent protein (GFP)/puro ($n=3$). (**b**) Representative cytospin preparations of bone marrow (BM) cells obtained from morbid MEs/G12V and MEs/puro mice. The cells were stained with Wright-Giemsa. Original magnification 200×; Scale bars 30 μm. (**c**) Representative histopathologic images of thymus obtained from the GFP/G12V mouse. A paraffin section of the thymus was stained with hematoxylin and eosin (H&E). Original magnification, ×40; vertical and horizontal scale bars, 1 cm and 200 μm, respectively. (**d**) Immunophenotype of BM and thymic (Th) cells obtained from representative morbid MEs/G12V and GFP/G12V mice. The dot plots show each surface antigen labeled with a corresponding monoclonal antibody versus expression of GFP or CD4. Ly5.1, CD11b, CD4, and c-Kit and CD8 were labeled with phycoerythrin (PE)-conjugated and allophycocyanin (APC)-conjugated monoclonal antibodies, respectively.

(and GFP) led to thymoma, sometimes together with leukocytosis, with a long latency (Figures 5a, c and d, and Table 1). In addition, to examine the possibility that the phenotypes associated with STAT5A#2 might change, similar to oncogenic *NRAS*, the BM cells transduced with STAT5A#2 (in pMYs-IRES-EGFP) and/or *MLL-SEPT6* (in pMXs-neo) were again transplanted into recipient mice under sublethal conditioning. Within an observation period of 160 days, two of three neo/#2 mice under sublethal conditioning died with longer latencies (134 and 139 days) and showed the same phenotype of myeloid hyperplasia in the BM, where a small population (15%) expressed STAT5A#2, although these had different phenotypes of pancytopenia and splenomegaly (Supplementary Figure 3b and data not shown). In contrast, two of three MS6/#2 mice and all of the three MS6/GFP mice survived and showed no hematological abnormalities in the peripheral blood, whereas one of the MS6/#2 mice died (125 day) but could not be analyzed because of post-mortem change, within the observation period. Histopathological analysis of one MS6/#2 mouse, which was killed 150 days after the transplantation, showed no significant hepatosplenomegaly but mild myeloid hyperplasia in the BM (data not shown). Only 30% of the BM cells were positive for donor-derived Ly-5.1, and 7% of the BM cells were positive for GFP, indicating expression of STAT5A#2 (Supplementary Figure 3c), whereas reverse transcriptase-PCR analysis of the BM cells gave very weak signals of *MLL-SEPT6* after 30 cycles (data not shown), but clearly visible signals after 35 cycles (Supplementary Figure 3c). Therefore, sublethal conditioning seemed to be inappropriate for leukemogenesis assays using oncogenes, such as *MLL-SEPT6* and STAT5A#2, which had relatively weak oncogenic potential in comparison with *MLL-ENL* and *NRAS*^{G12V}.

Finally, we examined whether *Hoxa9* may be involved in cooperation between the *MLL* fusion protein and oncogenic *NRAS in vivo*, such as in transformation assays *in vitro*. The leukemogenesis assays using the BM cells transduced with

Hoxa9 and oncogenic *NRAS* were carried out under lethal conditioning, because preliminary leukemogenesis assays under sublethal conditioning were unsuccessful probably because of engraftment failure (data not shown). The combination of *Hoxa9* and $NRAS^{G12V}$ (A9/G12V) led to death with short latencies (28 ± 7.5 days) (Figure 6a and Table 1), whereas *Hoxa9* (and GFP) *per se* induced no lethal disease within 120 days, as reported earlier.[37] The A9/G12V mice showed remarkable hepatosplenomegaly and had a tendency toward leukocytosis, anemia and thrombocytopenia (Table 1). Histopathological and immunophenotyping analyses of the BM cells revealed that the A9/G12V mice had a few, but prominent, myelomonocytic blasts (Figure 6b), with high expression of CD11b and Gr-1, and low level of c-Kit (Figure 6c). A Southern blot analysis of genomic DNAs derived from the spleens of the A9/G12V mice gave oligoclonal bands (data not shown). These results indicated that *Hoxa9* cooperated with oncogenic *NRAS* to rapidly induce lethal myeloid malignancy that was not identical but similar to the acute leukemia induced by *MLL* fusion proteins and oncogenic *NRAS*.

Taken together, these results *in vivo* suggested that *MLL* fusion proteins rapidly induce acute leukemia together with activated *NRAS*, at least in part through aberrant expression of *Hoxa9*.

Discussion

The present study provides several evidences that *MLL*-fusion-mediated leukemogenesis cooperated synergistically with Ras activation, but not with STAT5 activation. Although all known *MLL* fusion proteins were not tested in this study, we showed that this synergistic cooperation was not limited to the specific *MLL* fusion, using two different well-characterized types of *MLL* fusion proteins. In the light of the role of FLT3 mutations in *MLL*-fusion-mediated leukemogenesis described earlier,[6] signaling pathways downstream of FLT3 mutations were analyzed in the transfectants of HF6, a cell line expressing *MLL-SEPT6*. The immortalized cells, such as HF6 and A9G, used in this study might have acquired additional mutations. However, the phenotypes including IL-3 dependency, expression patterns of lineage markers and growth rates were not changed since their establishment (data not shown), thus suggesting that at least no mutations leading to critical transformation had occurred in these cell lines. Although recent studies have disclosed the differences in activation of signal molecules, including MAPK and STAT5, between *FLT3*-TKD and *FLT3*-ITD,[24,38] our experiments using transduction with FLT3 mutants and inhibition of the signal molecules first showed a crucial role of activation of MAPK rather than STAT5 in the factor-independent survival and proliferation of HF6 cells. Next, the myeloid transformation assays *in vitro* revealed that the activation of Raf-1, as well as oncogenic *NRAS*, transformed HF6 cells, but that constitutively active mutants (1*6 and #2) of STAT5A did not. The leukemogenesis assays *in vivo* also showed that oncogenic *NRAS* rapidly induced acute leukemia together with *MLL* fusion proteins, which differed from the original phenotype induced by each molecule. In contrast, the active STAT5A mutant did not confer obvious synergistic effects on the *MLL*-fusion-mediated leukemogenesis. Thus, these results *in vitro* and *in vivo* suggested that activation of the Ras/Raf/MAPK pathway may be sufficient for the transformation of HF6 cells and development of *MLL*-fusion-mediated leukemia.

Oncogenic *NRAS* induced thymoma in the leukemogenesis assays under sublethal conditioning, which is consistent with the

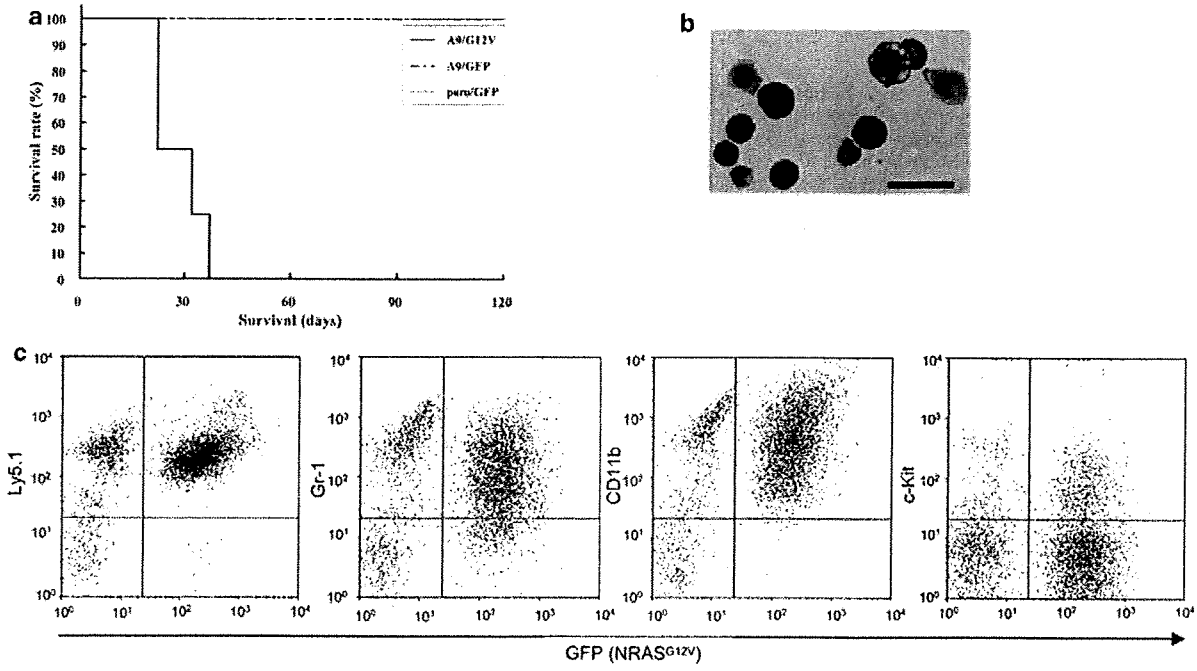

Figure 6 Leukemogenesis induced by *Hoxa9* and oncogenic neuroblastoma RAS viral (v-ras) oncogene homolog (*NRAS*) under lethal conditioning. (**a**) Survival curves of mice transplanted with *Hoxa9* and $NRAS^{G12V}$ (A9/G12V; $n=4$), A9/green fluorescent protein (GFP) ($n=6$) and puro/GFP ($n=3$). (**b**) Representative cytospin preparations of bone marrow (BM) cells obtained from morbid A9/G12V mice. The cells were stained with Wright-Giemsa. Original magnification, × 200; scale bar, 30 μm. (**c**) Immunophenotype of BM cells obtained from representative morbid A9/G12V mice. The dot plots show each surface antigen labeled with a corresponding monoclonal antibody versus expression of GFP. Ly5.1, Gr-1, CD11b, and c-Kit were labeled with phycoerythrin (PE)-conjugated and allophycocyanin (APC)-conjugated monoclonal antibodies, respectively.

development of T-lymphoma by *FLT3*-TKD in our experimental system (Ono *et al.*, unpublished data), whereas it led to the development of BM aplasia in our leukemogenesis assays under lethal conditioning. This difference in the disease phenotypes implies that forced expression of oncogenic *NRAS* in BM progenitors might be involved in its inhibitory effects on the engraftment of radioprotective cells as well as the antiproliferative effect of oncogenic *NRAS* in the early phase of the transplantation.[39] These disease phenotypes were also different from the development of MPD in the earlier reports.[39,40] This discrepancy might be due to the differences in the experimental systems, such as the retroviral transduction and mice strains. Meanwhile, the BM progenitors transduced with *Hoxa9* and $NRAS^{G12V}$ seemed to result in engraftment failure under sublethal conditioning, but these rapidly developed myeloid malignancy under lethal conditioning. A recent study using BM transplantation showed the possibility of drastic fluctuation in the engraftment of donor cells receiving pathological modification under sublethal conditioning;[41] hence, our unsuccessful results under sublethal conditioning might be associated with some instability of the transplantation.

Our leukemogenesis assays showed a definitively synergistic cooperation between *MLL* fusion proteins and oncogenic *NRAS* in the acceleration of disease onset and change of the phenotypes. Interestingly, the synergistic cooperation between *MLL* fusion proteins and Ras/Raf/MAPK activation closely correlated with recent clinical studies reporting the frequent coincidence of *MLL* fusion genes and mutations of *RAS*[20] or *RAF*.[42] It was reported that the additional expression of oncogenic *KRAS* induced an acute promyelocytic leukemia-like disease in transgenic mice expressing promyelocytic leukemia/retinoic acid receptor-α with an increased penetrance and decreased latency, although neither the penetrance nor the latency was significantly different from those in mice that died of MPD by expression of oncogenic *KRAS* alone.[43] Other groups recently reported that the combination of oncogenic *NRAS* and *MLL-AF9*[44] or *MLL-ENL*[45] is capable of developing *AML*, and that induced repression of oncogenic *NRAS* on the combination reverted *AML* to MPD by the *MLL* fusion gene (*MLL-AF9*) alone.[44] Although our findings that *MLL* fusion proteins and oncogenic *NRAS* cooperate to induce *AML* confirmed these notions, the present study further analyzed the involvement of *Hoxa9* and Raf, downstream of the cooperation between *MLL* fusion proteins and oncogenic *NRAS*. The myeloid transformation assays *in vitro* showed that the activation of Raf-1, as well as oncogenic *NRAS*, transformed A9G, a cell line expressing *Hoxa9*. The leukemogenesis assays *in vivo* also showed that *Hoxa9* and oncogenic *NRAS* rapidly developed myeloid malignancy. These results *in vitro* and *in vivo* suggested that, as downstream molecules, *Hoxa9* and Raf may have important roles in the synergistic leukemogenesis by *MLL* fusion proteins and oncogenic *NRAS*.

Our findings suggest a possible model of *MLL*-fusion-mediated leukemogenesis that was essentially recapitulated by *Hoxa9* expression and Ras/Raf/MAPK activation (Figure 7). In the context of secondary genetic alterations, such as *FLT3* mutations, this model explains the clinical features of acute leukemia with 11q23 translocations. First, overexpression, as well as TKD mutations, of *FLT3* frequently detected in the *MLL*-rearranged infant acute leukemia may be involved in the leukemogenesis mainly through activation of Ras/Raf/MAPK, because several studies reported that the signaling pathway of wild-type *FLT3* is similar to *FLT3*-TKD rather than *FLT3*-ITD.[24,38] Second, besides *FLT3*, other unknown molecular pathways that lead to the activation of Ras/Raf/MAPK might also be involved in the *MLL*-rearranged leukemia carrying no known genetic alterations, as *FLT3* alterations are not found very frequently in most *MLL*-rearranged leukemia except in infants.[46,47] Meanwhile, in the context of *MLL* fusion proteins, we analyzed the role of the *Hoxa9*-mediated pathway leading to leukemogenesis. Recent studies revealed that one of the *Hox*-cofactor molecules, *Meis1*, is an essential molecule involved in normal hematopoiesis[48] as well as *Hoxa9*-mediated leukemogenesis.[49] However, our experimental system[6] using BM cells transduced with *MLL* fusion proteins did not detect any significant upregulation of *Meis1* in comparison with the mock transduction as reported earlier,[50] in contrast with the findings by other groups.[14] Therefore, we focused on *Hoxa9*, one of the key molecules directly upregulated by *MLL* fusion proteins. Interestingly, a recent study showed that the combination of *Hoxa9* and *Meis1* cooperated with *Trib1*, which enhanced the phosphorylation of ERK, to induce acute leukemia in the BM transplantation assays.[51] Their study is not inconsistent with our findings; thus, the *HOX* and Ras/Raf/MAPK axes may have central roles in the molecular network of *MLL*-mediated leukemogenesis, which might be additively affected by other pathways, such as activation of STAT5 (Figure 7). In addition, at least, endogenous expression of *Meis1* in A9G cells is also considered to be important in this network, but further analysis will be required to clarify the role of *Meis1* in the collaboration between *HOX* and MAPK axes.

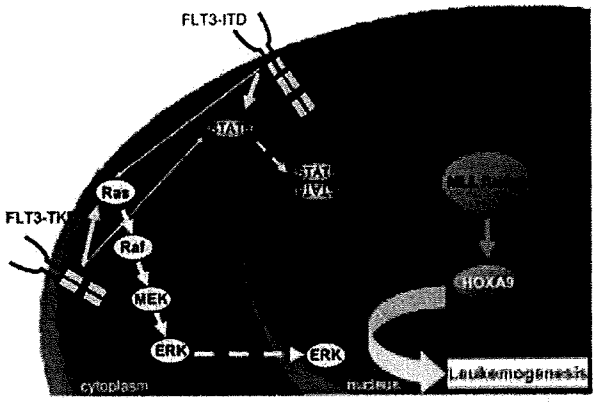

Figure 7 A model of *mixed-lineage-leukemia* (*MLL*)-mediated leukemogenesis together with secondary genetic alterations. *MLL* fusion protein and secondary genetic alterations cooperate to induce acute leukemia through synergistic molecular crosstalk between aberrant expression of *Hox* genes, including *Hoxa9*, and the activation of Ras/Raf/mitogen-activated protein kinase (MAPK). Other signaling pathways, including signal transducer and activator of transcription 5 (STAT5) activation, only additively affect the leukemogenic potential.

Conclusion

This study suggests that *MLL* fusion proteins synergistically cooperate with Ras/Raf/MAPK activation in leukemogenesis, at least partly through the upregulation of *Hoxa9*. Future studies analyzing the molecular crosstalk between *Hoxa9* and the Ras/Raf/MAPK cascade are expected to provide novel insights into the molecular mechanism of *MLL*-fusion-mediated leukemogenesis.

Conflict of interest

The authors declare no conflict of interest.

Acknowledgements

We thank Dr Guy Sauvageau (Laboratory of Molecular Genetics of Stem Cells, Institute for Research in Immunology and Cancer, Canada) for the plasmid harboring a fragment of *Hoxa9*, and Dr Yusuke Satoh (Hematology and Oncology, Osaka University Graduate School of Medicine, Osaka, Japan) for technical advice. We are also grateful to R&D Systems for providing cytokines, and Brian Quinn for language assistance. This work was supported in part by Chugai Pharmaceutical Company Ltd, Grants-in-Aid from the Ministry of Education, Culture, Sports, Science, and Technology in Japan, the Novartis Foundation (Japan) for the Promotion of Science and the Japan Leukaemia Research Fund.

References

1 Vogelstein B, Kinzler KW. Cancer genes and the pathways they control. *Nat Med* 2004; **10**: 789–799.
2 Look AT. Oncogenic transcription factors in the human acute leukemias. *Science* 1997; **278**: 1059–1064.
3 Rowley JD. The critical role of chromosome translocations in human leukemias. *Annu Rev Genet* 1998; **32**: 495–519.
4 Gilliland DG, Tallman MS. Focus on acute leukemias. *Cancer Cell* 2002; **1**: 417–420.
5 Kelly LM, Kutok JL, Williams IR, Boulton CL, Amaral SM, Curley DP *et al.* PML/RARalpha and FLT3-ITD induce an APL-like disease in a mouse model. *Proc Natl Acad Sci USA* 2002; **99**: 8283–8288.
6 Ono R, Nakajima H, Ozaki K, Kumagai H, Kawashima T, Taki T *et al.* Dimerization of MLL fusion proteins and FLT3 activation synergize to induce multiple-lineage leukemogenesis. *J Clin Invest* 2005; **115**: 919–929.
7 Schessl C, Rawat VP, Cusan M, Deshpande A, Kohl TM, Rosten PM *et al.* The *AML1-ETO* fusion gene and the FLT3 length mutation collaborate in inducing acute leukemia in mice. *J Clin Invest* 2005; **115**: 2159–2168.
8 Stubbs MC, Kim YM, Krivtsov AV, Wright RD, Feng Z, Agarwal J *et al.* MLL-AF9 and FLT3 cooperation in acute myelogenous leukemia: development of a model for rapid therapeutic assessment. *Leukemia* 2008; **22**: 66–77.
9 Watanabe-Okochi N, Kitaura J, Ono R, Harada H, Harada Y, Komeno Y *et al.* AML1 mutations induced MDS and MDS/AML in a mouse BMT model. *Blood* 2008; **111**: 4297–4308.
10 Ayton PM, Cleary ML. Molecular mechanisms of leukemogenesis mediated by MLL fusion proteins. *Oncogene* 2001; **20**: 5695–5707.
11 Meyer C, Kowarz E, Hofmann J, Renneville A, Zuna J, Trka J *et al.* New insights to the MLL recombinome of acute leukemias. *Leukemia* 2009; **23**: 1490–1499.
12 Yokoyama A, Somervaille TC, Smith KS, Rozenblatt-Rosen O, Meyerson M, Cleary ML. The menin tumor suppressor protein is an essential oncogenic cofactor for MLL-associated leukemogenesis. *Cell* 2005; **123**: 207–218.
13 Daser A, Rabbitts TH. Extending the repertoire of the *mixed-lineage leukemia* gene *MLL* in leukemogenesis. *Genes Dev* 2004; **18**: 965–974.
14 Hess JL. MLL: a histone methyltransferase disrupted in leukemia. *Trends Mol Med* 2004; **10**: 500–507.
15 Corral J, Lavenir I, Impey H, Warren AJ, Forster A, Larson TA *et al.* An *MLL-AF9* fusion gene made by homologous recombination causes acute leukemia in chimeric mice: a method to create fusion oncogenes. *Cell* 1996; **85**: 853–861.
16 Drynan LF, Pannell R, Forster A, Chan NM, Cano F, Daser A *et al.* MLL fusions generated by Cre-loxP-mediated *de novo* translocations can induce lineage reassignment in tumorigenesis. *EMBO J* 2005; **24**: 3136–3146.
17 Wang J, Iwasaki H, Krivtsov A, Febbo PG, Thorner AR, Ernst P *et al.* Conditional *MLL-CBP* targets GMP and models therapy-related myeloproliferative disease. *EMBO J* 2005; **24**: 368–381.
18 Chen W, Li Q, Hudson WA, Kumar A, Kirchhof N, Kersey JH. A murine *MLL-AF4* knock-in model results in lymphoid and myeloid deregulation and hematologic malignancy. *Blood* 2006; **108**: 669–677.
19 Taketani T, Taki T, Sugita K, Furuichi Y, Ishii E, Hanada R *et al.* FLT3 mutations in the activation loop of tyrosine kinase domain are frequently found in infant ALL with *MLL* rearrangements and pediatric ALL with hyperdiploidy. *Blood* 2004; **103**: 1085–1088.
20 Liang DC, Shih LY, Fu JF, Li HY, Wang HI, Hung IJ *et al.* K-Ras mutations and N-Ras mutations in childhood acute leukemias with or without mixed-lineage leukemia gene rearrangements. *Cancer* 2006; **106**: 950–956.
21 Gilliland DG, Griffin JD. The roles of FLT3 in hematopoiesis and leukemia. *Blood* 2002; **100**: 1532–1542.
22 Armstrong SA, Staunton JE, Silverman LB, Pieters R, den Boer ML, Minden MD *et al.* *MLL* translocations specify a distinct gene expression profile that distinguishes a unique leukemia. *Nat Genet* 2002; **30**: 41–47.
23 Murata K, Kumagai H, Kawashima T, Tamitsu K, Irie M, Nakajima H *et al.* Selective cytotoxic mechanism of GTP-14564, a novel tyrosine kinase inhibitor in leukemia cells expressing a constitutively active Fms-like tyrosine kinase 3 (FLT3). *J Biol Chem* 2003; **278**: 32892–32898.
24 Choudhary C, Schwable J, Brandts C, Tickenbrock L, Sargin B, Kindler T *et al.* AML-associated Flt3 kinase domain mutations show signal transduction differences compared with Flt3 ITD mutations. *Blood* 2005; **106**: 265–273.
25 Nosaka T, Kawashima T, Misawa K, Ikuta K, Mui AL, Kitamura T. STAT5 as a molecular regulator of proliferation, differentiation and apoptosis in hematopoietic cells. *EMBO J* 1999; **18**: 4754–4765.
26 Schubbert S, Shannon K, Bollag G. Hyperactive Ras in developmental disorders and cancer. *Nat Rev Cancer* 2007; **7**: 295–308.
27 Ariyoshi K, Nosaka T, Yamada K, Onishi M, Oka Y, Miyajima A *et al.* Constitutive activation of STAT5 by a point mutation in the SH2 domain. *J Biol Chem* 2000; **275**: 24407–24413.
28 Onishi M, Nosaka T, Misawa K, Mui AL, Gorman D, McMahon M *et al.* Identification and characterization of a constitutively active STAT5 mutant that promotes cell proliferation. *Mol Cell Biol* 1998; **18**: 3871–3879.
29 Kitamura T, Koshino Y, Shibata F, Oki T, Nakajima H, Nosaka T *et al.* Retrovirus-mediated gene transfer and expression cloning: powerful tools in functional genomics. *Exp Hematol* 2003; **31**: 1007–1014.
30 Kroon E, Krosl J, Thorsteinsdottir U, Baban S, Buchberg AM, Sauvageau G. Hoxa9 transforms primary bone marrow cells through specific collaboration with Meis1a but not Pbx1b. *EMBO J* 1998; **17**: 3714–3725.
31 Sakaue-Sawano A, Kurokawa H, Morimura T, Hanyu A, Hama H, Osawa H *et al.* Visualizing spatiotemporal dynamics of multicellular cell-cycle progression. *Cell* 2008; **132**: 487–498.
32 Calvo KR, Sykes DB, Pasillas M, Kamps MP. Hoxa9 immortalizes a granulocyte-macrophage colony-stimulating factor-dependent promyelocyte capable of biphenotypic differentiation to neutrophils or macrophages, independent of enforced meis expression. *Mol Cell Biol* 2000; **20**: 3274–3285.
33 Ono R, Ihara M, Nakajima H, Ozaki K, Kataoka-Fujiwara Y, Taki T *et al.* Disruption of *Sept6*, a fusion partner gene of *MLL*, does not affect ontogeny, leukemogenesis induced by *MLL-SEPT6*, or phenotype induced by the loss of *Sept4*. *Mol Cell Biol* 2005; **25**: 10965–10978.
34 Nosaka T, van Deursen JM, Tripp RA, Thierfelder WE, Witthuhn BA, McMickle AP *et al.* Defective lymphoid development in mice lacking Jak3. *Science* 1995; **270**: 800–802.
35 Moriggl R, Gouilleux-Gruart V, Jähne R, Berchtold S, Gartmann C, Liu X *et al.* Deletion of the carboxyl-terminal transactivation domain of MGF-STAT5 results in sustained DNA binding and a dominant negative phenotype. *Mol Cell Biol* 1996; **16**: 5691–5700.
36 Schwaller J, Parganas E, Wang D, Cain D, Aster JC, Williams IR *et al.* STAT5 is essential for the myelo- and lymphoproliferative disease induced by TEL/JAK2. *Mol Cell* 2000; **6**: 693–704.
37 Nakamura T, Largaespada DA, Shaughnessy Jr JD, Jenkins NA, Copeland NG. Cooperative activation of Hoxa and Pbx1-related genes in murine myeloid leukaemias. *Nat Genet* 1996; **12**: 149–153.
38 Grundler R, Miething C, Thiede C, Peschel C, Duyster J. FLT3-ITD and tyrosine kinase domain mutants induce 2 distinct phenotypes in a murine bone marrow transplantation model. *Blood* 2005; **105**: 4792–4799.

39 MacKenzie KL, Dolnikov A, Millington M, Shounan Y, Symonds G. Mutant N-ras induces myeloproliferative disorders and apoptosis in bone marrow repopulated mice. *Blood* 1999; **93**: 2043–2056.
40 Parikh C, Subrahmanyam R, Ren R. Oncogenic NRAS rapidly and efficiently induces CMML- and AML-like diseases in mice. *Blood* 2006; **108**: 2349–2357.
41 Santaguida M, Schepers K, King B, Sabnis AJ, Forsberg EC, Attema JL *et al.* JunB protects against myeloid malignancies by limiting hematopoietic stem cell proliferation and differentiation without affecting self-renewal. *Cancer Cell* 2009; **15**: 341–352.
42 Christiansen DH, Andersen MK, Desta F, Pedersen-Bjergaard J. Mutations of genes in the receptor tyrosine kinase (RTK)/RAS-BRAF signal transduction pathway in therapy-related myelodysplasia and acute myeloid leukemia. *Leukemia* 2005; **19**: 2232–2240.
43 Chan IT, Kutok JL, Williams IR, Cohen S, Moore S, Shigematsu H *et al.* Oncogenic K-ras cooperates with PML-RAR alpha to induce an acute promyelocytic leukemia-like disease. *Blood* 2006; **108**: 1708–1715.
44 Kim WI, Matise I, Diers MD, Largaespada DA. RAS oncogene suppression induces apoptosis followed by more differentiated and less myelosuppressive disease upon relapse of acute myeloid leukemia. *Blood* 2009; **113**: 1086–1096.
45 Zuber J, Radtke I, Pardee TS, Zhao Z, Rappaport AR, Luo W *et al.* Mouse models of human AML accurately predict chemotherapy response. *Genes Dev* 2009; **23**: 877–889.
46 Chillon MC, Fernandez C, Garcia-Sanz R, Balanzategui A, Ramos F, Fernandez-Calvo J *et al.* FLT3-activating mutations are associated with poor prognostic features in AML at diagnosis but they are not an independent prognostic factor. *Hematol J* 2004; **5**: 239–246.
47 Bacher U, Haferlach C, Kern W, Haferlach T, Schnittger S. Prognostic relevance of FLT3-TKD mutations in AML: the combination matters–an analysis of 3082 patients. *Blood* 2008; **111**: 2527–2537.
48 Hisa T, Spence SE, Rachel RA, Fujita M, Nakamura T, Ward JM *et al.* Hematopoietic, angiogenic and eye defects in Meis1 mutant animals. *EMBO J* 2004; **23**: 450–459.
49 Wong P, Iwasaki M, Somervaille TC, So CW, Cleary ML. Meis1 is an essential and rate-limiting regulator of MLL leukemia stem cell potential. *Genes Dev* 2007; **21**: 2762–2774.
50 Horton SJ, Grier DG, McGonigle GJ, Thompson A, Morrow M, De Silva I *et al.* Continuous MLL-ENL expression is necessary to establish a 'Hox Code' and maintain immortalization of hematopoietic progenitor cells. *Cancer Res* 2005; **65**: 9245–9252.
51 Jin G, Yamazaki Y, Takuwa M, Takahara T, Kaneko K, Kuwata T *et al.* Trib1 and Evi1 cooperate with Hoxa and Meis1 in myeloid leukemogenesis. *Blood* 2007; **109**: 3998–4005.

Supplementary Information accompanies the paper on the Leukemia website (http://www.nature.com/leu)

Leukemia (2010) 24, 1018–1024

www.nature.com/leu

ORIGINAL ARTICLE

AID-induced T-lymphoma or B-leukemia/lymphoma in a mouse BMT model

Y Komeno[1,2], J Kitaura[1,2], N Watanabe-Okochi[3,4], N Kato[1,2], T Oki[1,2], F Nakahara[1,2], Y Harada[5], H Harada[6], R Shinkura[7], H Nagaoka[7], Y Hayashi[8], T Honjo[7] and T Kitamura[1,2]

[1]Division of Cellular Therapy, Advanced Clinical Research Center, Institute of Medical Science, University of Tokyo, Minato-ku, Tokyo, Japan; [2]Division of Stem Cell Signaling, Center for Stem Cell Therapy, Institute of Medical Science, University of Tokyo, Minato-ku, Tokyo, Japan; [3]Department of Hematology and Oncology, Graduate School of Medicine, University of Tokyo, Bunkyo-ku, Tokyo, Japan; [4]Department of Transfusion Medicine, Graduate School of Medicine, University of Tokyo, Bunkyo-ku, Tokyo, Japan; [5]International Radiation Information Center, Research Institute for Radiation Biology and Medicine, Hiroshima University, Minami-ku, Hiroshima, Japan; [6]Department of Hematology and Oncology, Research Institute for Radiation Biology and Medicine, Hiroshima University, Minami-ku, Hiroshima, Japan; [7]Department of Immunology and Genomic Medicine, Graduate School of Medicine, Kyoto University, Sakyo-ku, Kyoto, Japan and [8]Department of Hematology/Oncology, Gunma Children's Medical Center, Shibukawa, Gunma, Japan

Activation-induced cytidine deaminase (AID) diversifies immunoglobulin through somatic hypermutation (SHM) and class-switch recombination (CSR). AID-transgenic mice develop T-lymphoma, indicating that constitutive expression of AID leads to tumorigenesis. Here, we transplanted mouse bone marrow cells transduced with AID. Twenty-four of the 32 recipient mice developed T-lymphoma 2–4 months after the transplantation. Surprisingly, unlike AID-transgenic mice, seven recipients developed B-leukemia/lymphoma with longer latencies. None of the mice suffered from myeloid leukemia. When we used nude mice as recipients, they developed only B-leukemia/lymphoma, presumably due to lack of thymus. Analysis of AID mutants suggested that an intact form with SHM activity is required for maximum ability of AID to induce lymphoma. Except for a K-ras active mutant in one case, specific mutations could not be identified in T-lymphoma; however, Notch1 was constitutively activated in most cases. Importantly, truncations of Ebf1 or Pax5 were observed in B-leukemia/lymphoma. In conclusion, this is the first report on the potential of AID overexpression to promote B-cell lymphomagenesis in a mouse model. Aberrant expression of AID in bone marrow cells induced leukemia/lymphoma in a cell-lineage–dependent manner, mainly through its function as a mutator.
Leukemia (2010) **24**, 1018–1024; doi:10.1038/leu.2010.40;
published online 1 April 2010
Keywords: AID; BMT; T-lymphoma; B-leukemia/lymphoma

Introduction

Under physiological conditions, activation-induced cytidine deaminase (AID) is expressed in germinal center (GC) B-cells and initiates somatic hypermutation (SHM) and class-switch recombination (CSR) by deaminating a cytosine to create a uracil.[1,2] Structurally, the N-terminal or C-terminal domain of AID is indispensable for SHM or CSR, respectively.[3–5] Interestingly, expression of AID is increased in B-lymphoid leukemia or GC-derived B-lymphoma, with frequent hypermutation of proto-oncogenes and reciprocal chromosomal translocation.[6–9] In fact, recent studies have shown that AID is required for GC-derived lymphomagenesis and c-Myc/IgH chromosomal translocations.[10,11] In addition, elevated expression of endogenous AID and aberrant somatic mutations in tumor-related genes have also been observed in cancerous tissues related to inflammation.[12] Analysis of AID-transgenic (Tg) mice has revealed that constitutive expression of AID leads to tumorigenesis; ubiquitous and constitutive expression of AID induced lethal T-lymphoma with no apparent chromosomal translocation, occasionally accompanied by lung, liver, and gastric cancers,[13,14] and specific expression of AID in double-positive thymocytes also induced T-lymphoma.[15] However, neither AID-Tg mice specifically expressing AID in single-positive thymocytes and mature T-cells nor AID-Tg mice with CD19$^+$ B-cell-specific expression of AID developed lymphoma/leukemia.[15,16] These results suggest that susceptibility to AID-induced tumorigenesis depends on tissue or cell lineage, but the underlying mechanism remains obscure. Importantly, sequencing analysis in AID-Tg mice indicated that AID is an organ-specific mutator of non-Ig genes.[14] To prevent accumulation of unfavorable mutations induced by AID, its activity is tightly regulated by several mechanisms.[17]

In this study, we focused on AID-mediated leukemogenesis and created a mouse bone marrow transplantation (BMT) model, using BM cells retrovirally transduced with AID. Notably, recipient mice developed B-leukemia/lymphoma, albeit less frequently as compared with thymic T-lymphoma.

Correspondence: Dr T Kitamura, Division of Cellular Therapy, Advanced Clinical Research Center, Institute of Medical Science, University of Tokyo, 4-6-1 Shirokanedai, Minato-ku, Tokyo 108-8639, Japan.
E-mail: kitamura@ims.u-tokyo.ac.jp
Received 23 November 2009; revised 8 January 2010; accepted 9 February 2010; published online 1 April 2010

Materials and methods

Retroviral constructs, transfection, and retrovirus production

Murine AID (mAID), mAID mutants (G23S[4] and Δ189–198[5]), human AID (hAID), and hAID mutants (P20[3] and JP8B[3]) were subcloned into the pMYsIG vector as described in 'Supplementary Materials and methods'. All constructs were verified by DNA sequencing. Expression of wild-type or mutant AID was recognized in 293T cells transiently transfected with each construct. Retroviruses were generated by transient transfection of Plat-E packaging cells with FuGene 6 (Roche Diagnostics, Mannheim, Germany), as described earlier.[18–20]

Mouse BMT

Mouse BMT was performed as described earlier.[20] C57BL/6 CD45.1 or CD45.2 mice were used as donors or recipients,

respectively. Infected cells (2×10^5) were intravenously injected into recipient mice, which had been administered a sublethal dose of γ-irradiation. Overall survival was estimated using the Kaplan–Meier method and log-rank test. Data are presented as the means ± s.d. PB smears and cytospin slides were stained with Hemacolor (Merck, Darmstadt, Germany). Tissues were fixed in 4% w/v buffered formalin, embedded in paraffin, and then sliced and stained with standard hematoxylin and eosin. All animal studies were approved by the Animal Care Committee of the Institute of Medical Science, The University of Tokyo.

Flow cytometric analysis

Cells were stained with phycoerythrin-conjugated monoclonal antibodies (eBiosciences, San Diego, CA, USA), as described.[20] Flow cytometric analysis was performed with a FACSCalibur equipped with CellQuest software (BD Biosciences, San Jose, CA, USA) and Flowjo software (Tree Star, San Carlos, CA, USA).

Western blotting

Equal numbers of cells were denatured in pre-heated sample buffer. Western blotting was performed as described.[20] Anti-AID mAb raised against the N-terminus of mAID, and anti-α-tubulin Ab (T6074, Sigma-Aldrich, St Louis, MO, USA) were used.

Southern blotting

Southern blotting was performed as described.[20] Briefly, 10 μg of genomic DNA digested with *EcoRI* was electrophoresed on a 0.7% agarose gel. Proviruses were probed with a ^{32}P-labeled GFP probe.

Reverse transcription and real-time PCR

Real-time PCR was performed using LightCycler (Roche Diagnostics), as described.[20] cDNA was amplified using a SYBR Premix EX Taq (Takara, Shiga, Japan). Primer pairs and conditions used for real-time PCR are listed in 'Supplementary Materials and methods'. Informed consent for the use of the human leukemia/lymphoma cells was obtained from patients in accordance with the Declaration of Helsinki, and study approval was obtained from the ethics committee of the Institute of Medical Science, the University of Tokyo (Approval Number 20-10-0620).

Sequencing of target genes

Genomic PCR was performed by using AmpliTaq Gold (Roche Molecular Systems Inc., Branchburg, NJ, USA) and the primer pairs described in 'Supplementary Materials and methods'. The PCR products were gel-purified and directly sequenced. If necessary, PCR products were subcloned and sequenced.

Treatment of AID-induced T-lymphoma cell lines with γ-secretase inhibitor

Cell lines of AID-induced T-lymphoma were established by culturing tumor cells in RPMI1640 with 20% FBS. Human T-acute lymphoblastic leukemia (T-ALL) cell lines Jurkat and HPB-ALL were cultured in RPMI1640 with 10% FBS. Various concentrations of γ-secretase inhibitor (DAPT, 565770, Calbiochem, Darmstadt, Germany) or vehicle (DMSO, Wako, Osaka, Japan) were added to 5×10^3 cells for 72 h. Cell growth was estimated by using CellTiter-Glo (Promega, Madison, WI, USA). Cleavage of intracellular domains of Notch1 (ICN) was detected by anti-ICN antibody (2421, Cell Signaling, Beverly, MA, USA) in western blotting.

Results

Transduction with AID into BM cells causes B-leukemia/lymphoma as well as thymic T-lymphoma in a mouse BMT model

First, we asked whether transduction of wild-type mAID (WT) into BM cells caused leukemia/lymphoma other than T-lymphoma in a BMT model ($n = 32$) (Figure 1). We confirmed efficient retrovirus infection: 50–70% and 76–84% of the BM cells transduced with WT or mock, respectively, were GFP-positive before transplantation. The recipient mice of WT-transduced cells developed thymic T-lymphoma more frequently than did AID-Tg mice[13] (75 vs 35%). The disease was associated with hepatosplenomegaly, killing the mice in 2–4 months after transplantation (Figure 1a; Supplementary Figure 1; Supplementary Table 1). Histological and flow cytometric analyses showed that the thymus was filled with the T-lymphoblastic cells $CD3^{dull}$, $CD4^+$, $CD8^+$, and $Thy1.2^+$, indicating the differentiation block at early stages of T-cell development in thymus (Figures 1b–d). The complete blood counts of these mice were usually normal, except for the increase of T-lymphoblastic cells or mature granulocytes in some cases (Supplementary Figure 1; Supplementary Table 1, and data not shown). Notably, 7 of 32 transplanted mice (22%) developed B-leukemia/lymphoma with pancytopenia and splenomegaly, and died with significantly longer latencies as compared with those of T-lymphoma (Figures 1a–d; Supplementary Figure 1; Supplementary Table 1). Spleen and BM were filled with B-lymphoblastic cells in most cases, while affected lymph nodes differed in size among cases. B-lymphoma cells were $B220^+$, $CD19^+$, $CD43^{dull/+}$, $c\text{-}kit^{dull/+}$, and IgM^- (Figure 1d). Neither Bcl-6 induction[21,22] nor abnormal Ikaros deletions[23] were detected in these cells (data not shown). There was a wide range of GFP-positive ratios among AID-induced T- or B-lymphoma cells, irrespective of disease severity (Supplementary Figure 2 and data not shown). Sequencing analysis of GFP gene integrated into the genome revealed multiple mutations, resulting in reduced green fluorescence. Interestingly, one recipient developed both T- and B-lymphoma. None of the mice suffered from myeloid leukemia. The lymphoma cells, irrespective of T- or B-lineage, were serially transplantable and developed T- or B-leukemia with shorter latencies, respectively (data not shown). The recipient mice of mock-transduced cells did not develop any leukemia/lymphoma (Figure 1a). Collectively, transduction with AID into BM cells led to thymic T-lymphoma or B-leukemia/lymphoma, but not myeloid leukemia in a mouse BMT model. Similar results were obtained when Balb/c mice were used (data not shown).

We next asked whether the integration of retroviruses influenced the different phenotypes (T- or B-lymphoma) in AID-induced leukemogenesis. Southern blot analysis demonstrated a single or several proviral integrations in T-lymphoma samples (Figure 1e, left panel). On the other hand, we found that a single integration was predominant in B-lymphoma samples (Figure 1e, right panel). In one recipient harboring both T- and B-lymphoma, a distinct integration was confirmed in each sample (Figure 1e, right panel, lanes *B and *T), indicating the double cancer in this case. We identified a single or several retroviral integration sites (RIS) from lymphoma samples by inverse PCR method (Supplementary Table 2). However, we could not find any specific relationship between RIS and different phenotypes of lymphomas. In addition, a common integration site was identified only in one recipient (ID69) (Supplementary Table 2). These results suggested that AID-induced lymphomagenesis mainly depended on its intrinsic function, but not RIS.

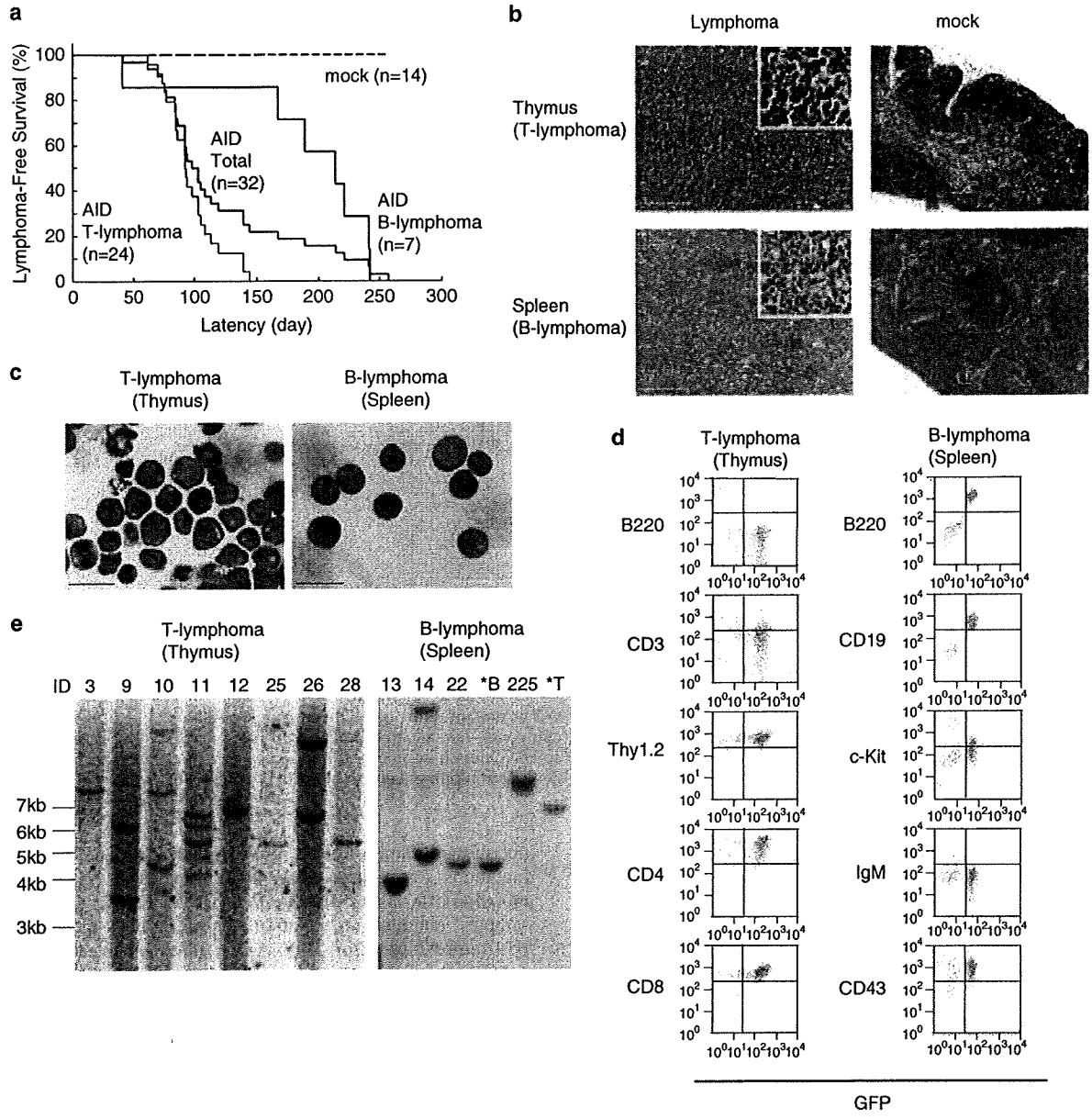

Figure 1 AID-induced T-lymphoma and B-leukemia/lymphoma in a mouse BMT model. (**a**) Kaplan–Meier plot of survival (black lines). Survival curve for AID recipient mice that developed T-lymphoma or B-lymphoma is indicated by green or red line, respectively. (**b**) Hematoxylin and eosin staining of AID-induced T-lymphoma (thymus, upper/left panel), control thymus (upper/right panel), AID-induced B-lymphoma (spleen, lower/left panel), or control spleen (lower/right panel). Magnifications × 200 (overview) and × 400 (insert). Scale bars: 200 μm. (**c**) Cytospin preparations of T-lymphoma (left panel) and B-lymphoma (right panel). Magnification × 1000. Scale bars: 20 μm. (**d**) Flow cytometric analysis of lymphoma cells. (**e**) Southern blotting of T-lymphoma (left panel) and B-lymphoma (right panel). *B or *T in the right panel indicates B- or T-lymphoma, respectively, which was found in the same mouse (ID 29).

We then asked whether other hematopietic malignancies, including myeloid leukemia, are induced in the absence of thymus. We used athymic nude mice as recipients of a BMT model, finding that 5 of 8 nude mice transplanted with AID-transduced BM cells developed B-leukemia/lymphoma, but no other hematopoietic diseases were observed (Supplementary Figure 3). Thus, B-leukemia/lymphoma was predominantly induced in the absence of thymus, but transduction of AID into BM cells did not induce myeloid leukemia. Altogether, these results suggested that the oncogenic transformation of AID-transduced BM cells requires *in vivo* environment suitable for differentiation and proliferation of immature lymphoid cells.

Impaired lymphomagenesis by SHM-defective AID mutants

To examine how SHM and/or CSR activities of AID contribute to lymphomagenesis, we constructed a BMT model using mutant forms of AID: missense mutant G23S with decreased SHM activity[4]; and truncation mutant Δ189–198 defective for CSR

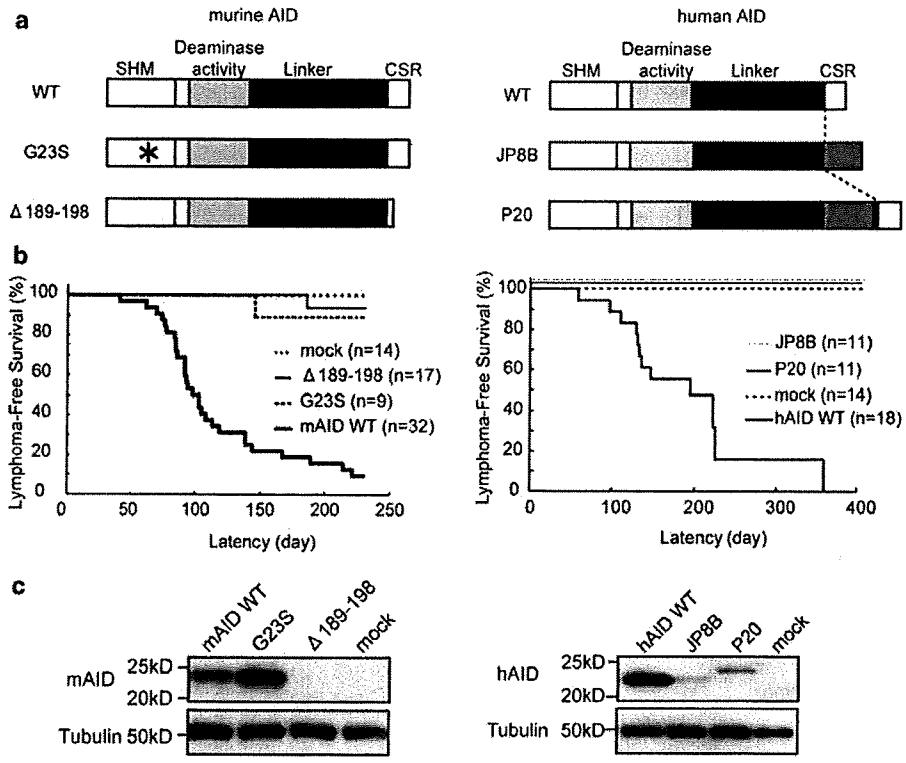

Figure 2 A BMT model using mutant forms of AID. (**a**) Diagrams of WT or mutant forms of AID. Left panel, mAID. G23S harbors a missense mutation (asterisk). Δ189–198 mutant lacks C-terminal 10 residues. Right panel, human AID (hAID). JP8B has a frameshift replacement of the C-terminus with 26 residues. P20 has an insertion of 34 residues. (**b**) Kaplan–Meier curves for the survival. Left panel, mAID. Right panel, hAID. (**c**) Expression of WT or mutant forms of AID in GFP-sorted BM cells by western blotting. Left panel, mAID. Right panel, hAID.

activity (Figure 2a, left panel).[5] Interestingly, recipients of these mutants showed a significantly decreased incidence of lymphoma as compared with those of WT (G23S $n=1/9$, 11%; Δ189–198 $n=1/17$, 6%) (Figure 2b, left panel). Each mutant developed only T-lymphoma. The expression level of G23S was comparable with that of WT in GFP-sorted BM cells (Figure 2c, left panel). On the other hand, the expression of Δ189–198 mutant in GFP-sorted BM cells was hardly detectable (Figure 2c, left panel). Similar results were obtained when hAID and its C-terminal mutants JP8B and P20 were transduced into BM cells (Figures 2a–c, right panels). Therefore, it was difficult to evaluate the effect of the CSR activity of AID on lymphomagenesis. Altogether, these results suggest that the intact form of AID with SHM activity is required to maximally exert its oncogenic activity.

An active mutation of K-ras in one case as well as multiple point mutations of Notch1, PTEN, and c-Myc was observed in AID-induced T-lymphoma

As point mutations are introduced into non-Ig genes such as *TCR* or *c-Myc* gene in T-lymphoma cells of AID-Tg mice,[13] we next asked which mutations caused by AID were responsible for T-lymphomagenesis in a mouse BMT model. On the basis of the fact that AID-mediated mutations occur after about 100 nucleotides downstream of the promoter and extend to 1–2 kb,[24] we performed genomic sequencing of several possible target genes in the region encompassing 0.5–1 kb from the transcription start site, in addition to the mutational hotspots implicated in tumorigenesis (Supplementary Table 3 and data not shown). Similar to the results on AID-Tg mice,[13] multiple mutations were observed in the *c-Myc* gene. An activating mutation of *K-ras* (G13D) was detected in 1 out of 14 analyzed samples, although no mutation was found in *N-ras*, *H-ras*, or *p53* tumor suppressor gene. As for genes involved in human T-ALL, *Notch1*[25] and *Pten*, but not *Fbxw7*, had multiple mutations. Intriguingly, we found several mutations in exon 27 (HD domain) and exon 34 (PEST domain), mutational hotspots of *Notch1* far downstream from the transcription start site. Consistent with the earlier report,[13] detected mutations were predominantly transition mutations and strongly biased to GC bases. Collectively, multiple mutations in T-lymphoma were introduced by AID, probably in association with lymphomagenesis.

Most AID-induced T-lymphoma cells exhibited constitutive activation of Notch1 and were susceptible to a γ-secretase inhibitor

The finding that Notch1 mutations were observed in AID-induced T-lymphoma led us to address the question of whether these mutations caused the activation of Notch1, leading to T-lymphomagenesis. Interestingly, western blot analysis demonstrated that cleavage of intracellular Notch1 (ICN) was evident in most T-lymphoma samples tested (Figure 3a), indicating that constitutive activation of Notch1 occurred in most T-lymphoma cells. In support of this finding, real-time PCR analysis showed increased expression of Hes1 and c-Myc and decreased expression of PTEN in most samples (Figure 3b). Expression levels of Notch1 did not significantly vary among these samples, except for a few cases. Interestingly, when we treated two cell

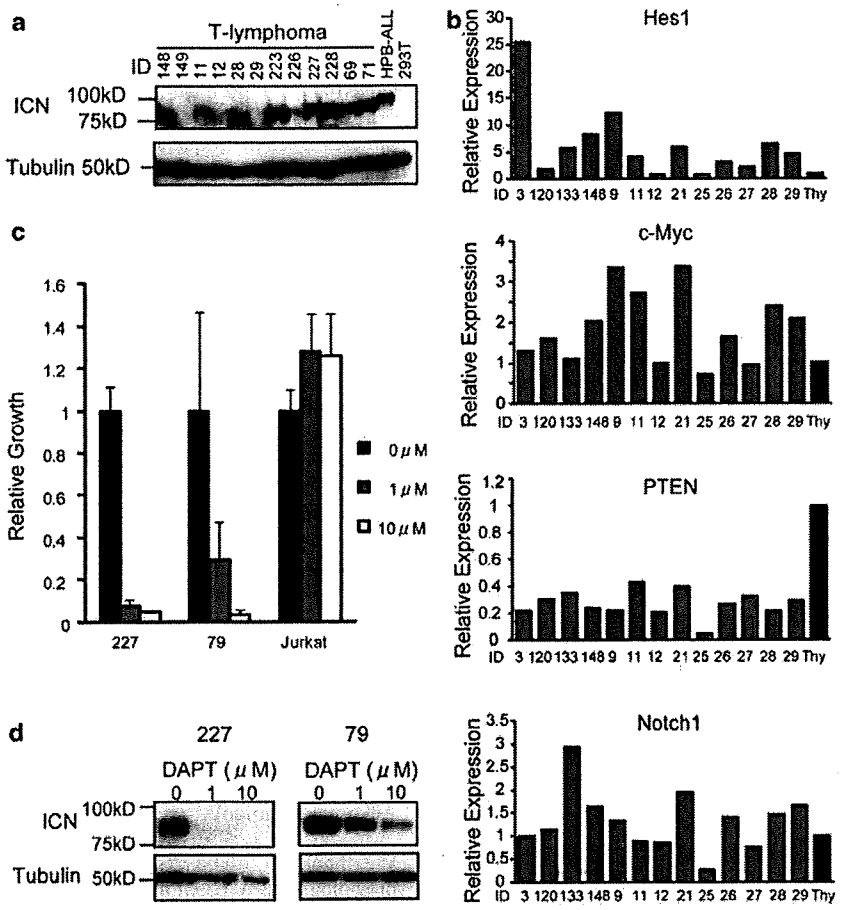

Figure 3 Notch1 is constitutively activated in AID-induced T-lymphoma. (**a**) Cleavage of intracellular Notch1 (ICN) in AID-induced T-lymphoma confirmed by western blotting. (**b**) Relative expression levels of Hes1, c-Myc, PTEN, or Notch1 in T-lymphoma samples and normal thymocytes (Thy) measured by real-time PCR. (**c**) The relative growth estimated by colorimetric assay. Two cell lines 227 and 79 established from AID-induced T-lymphoma, or Jurkat cells were treated with indicated concentrations of DAPT for 72 h. The means ± s.d. of triplicate measurements are shown. Data are representative of three independent experiments. (**d**) Cleavage of ICN examined by western blotting. Cells were treated as described in (**c**). Data are representative of three independent experiments.

lines established from AID-induced T-lymphoma with a γ-secretase inhibitor, DAPT, the growth as well as the cleavage of ICN of these cell lines was dose dependently inhibited by DAPT (Figures 3c and d). Although Notch1 mutations did not account for constitutive activation of Notch1 in all cases, these results indicated that T-lymphomagenesis in most cases was induced by Notch1 activation, probably in conjunction with AID-introduced mutations of the related genes.

Truncation mutations of Ebf1 and Pax5 were found in AID-induced B-lymphoma

To investigate the relevant mechanism of AID-induced B-lymphomagenesis, we performed genomic sequencing of the *Ebf1* and *Pax5* genes of AID-induced B-leukemia/lymphoma of seven recipient mice (Supplementary Table 4 and data not shown). Intriguingly, sequencing of *Ebf1* revealed a 23-base deletion and a 4-base insertion in exon 2, which together resulted in truncation in one sample. In addition, multiple point mutations were found in three samples. As for *Pax5*, we found a truncation caused by a couple of 2-base deletions and a point mutation in exon 1a in one case, and point mutations in two cases. On the basis of the recent study,[26] the aberrations of *Pax5* and *Ebf1* genes described above might have some function in B-lymphomagenesis in the recipient mice. On the other hand, we did not find c-Myc/IgH chromosomal translocations in B-lymphoma samples analyzed by PCR combined with Southern blotting (data not shown).[27] Collectively, these results suggested that B-lymphomagenesis in a BMT model was, at least in part, due to AID-introduced mutations/deletions of the genes regulating B-cell differentiation.

Discussion

In this study, we constructed a mouse BMT model to test whether AID is implicated in the pathogenesis of leukemia/lymphoma including myeloid leukemia. Our results revealed that aberrant expression of AID in BM cells led to T-lymphoma and less frequently B-leukemia/lymphoma, but not myeloid leukemia (Figure 1). The recipient mice developed 'thymic' T-lymphoma, but not 'peripheral type' T-lymphoma observed in 65% of AID-Tg mice.[13] It was noteworthy that B-leukemia/lymphoma was observed in our BMT model, but not in AID-Tg